Juliana Crestani Ribeiro de Souza

Spatial Distribution of Galactic Globular Clusters: Distance Uncertainties and Dynamical Effects

Porto Alegre

2017

Juliana Crestani Ribeiro de Souza

Spatial Distribution of Galactic Globular Clusters: Distance Uncertainties and Dynamical Effects

Dissertação elaborada sob orientação do Prof. Dr. Eduardo Luis Damiani Bica, co-orientação do Prof. Dr. Charles José Bonato e apresentada ao Instituto de Física da Universidade Federal do Rio Grande do Sul em preenchimento do requisito parcial para obtenção do título de Mestre em Física.

Porto Alegre
2017

Acknowledgements

To my parents, who supported me and made this possible, in a time and place where being in a university was just a distant dream. To my dearest friends Elisabeth, Robert, Augusto, and Natália - who so many times helped me go from "I give up" to "I'll try once more". To my cats Kira, Fen, and Demi - who lazily join me in bed at the end of the day, and make everything worthwhile.

"But, first of all, it will be necessary to explain what is our idea of a cluster of stars, and by what means we have obtained it. For an instance, I shall take the phenomenon which presents itself in many clusters: It is that of a number of lucid spots, of equal lustre, scattered over a circular space, in such a manner as to appear gradually more compressed towards the middle; and which compression, in the clusters to which I allude, is generally carried so far, as, by imperceptible degrees, to end in a luminous center, of a resolvable blaze of light."

William Herschel, 1789

Abstract

We provide a sample of 170 Galactic Globular Clusters (GCs) and analyse its spatial distribution properties. Using a comprehensive dust cloud catalogue, we list the GCs that are behind one or more identified dust clouds and could be subjected to a more complex extinction curve than extinction catalogues consider. Distance uncertainty values are gathered from recent literature and compared to values derived from an error propagation formula. GCs are grouped according to unusual characteristics, such as relatively young age or possible connection to dwarf galaxy nuclei, so that their effect on the general distribution can be isolated. Additionally, we compute the centroid of the GC distribution and study how it relates to the distance to the centre of the Galaxy. Considering that galactic formation via monolithic collapse is expected to be symmetrical, we probe asymmetries and how distance uncertainty values modify them. Spatial velocities and a Galactic potential are used to verify if any asymmetries in the spatial distribution are due to co-moving objects, or if they are merely transient effects.

Keywords: Galaxy: fundamental parameters, Galaxy: kinematics and dynamics, Globular Clusters: general.

Resumo

Fornecemos uma amostra de 170 Aglomerados Globulares Galácticos (GCs) e analisamos as propriedades de sua distribuição espacial. Utilizando um vasto catálogo de nuvens escuras identificadas, listamos os GCs que estão atrás de uma ou mais delas e que podem estar submetidos a uma extinção mais complexa do que a considerada por mapas de extinção. Valores de incerteza em distância são obtidos da literatura recente e comparados com valores derivados de uma fórmula de propagação de erro. GCs são agrupados de acordo com características inusitadas, tais como idades relativamente jovens ou possível conexão com núcleos de galáxias anãs, de forma que o efeito desses grupos pode ser isolado na distribuição espacial geral. Adicionalmente, computamos o centróide da distribuição de GCs e estudamos como esse se relaciona com a distância ao centro da Galáxia. Considerando que uma formação galáctica via colapso monolítico é supostamente simétrica, investigamos assimetrias e como os valores de incerteza das distâncias as modificam. Velocidades espaciais e um potencial Galáctico são empregados para verificar se quaisquer assimetrias na distribuição espacial são devidas a objetos em movimento coerente, ou se são somente efeitos transientes.

Palavras-chave: Galáxia: parâmetros fundamentais, Galáxia: cinemática e dinâmica, Aglomerados Globulares: geral.

Contents

1 INTRODUCTION 13
1.1 Historical Background 13
1.2 The Present Work 18
1.3 Objectives 20

2 DATA 23
2.1 Defining a Globular Cluster Catalogue 23
2.2 The Sample 24

3 INTERSTELLAR EXTINCTION 39
3.1 Dust Clouds 40

4 DISTANCE UNCERTAINTY ESTIMATES 49
4.1 Error Propagation 49
4.2 Uncertainty Values in the Literature 50

5 SUBSAMPLES 55
5.1 Retrograde, Young, and Related to Accretions 55
5.2 High and Low Metallicities 56
5.3 Small Heights from the Galactic Plane 56

6 DISTRIBUTION FUNCTIONS 59
6.1 Discrete Distribution 59
6.2 Continuous Distribution 60
6.3 Centroids and Shapes of the Distributions 60

7 RESULTS 63
7.1 Full Sample 63
7.2 High and Low Metallicities 66
7.3 Small Heights from the Galactic Plane 66
7.4 The x Direction Structure 66

7.4.1 General Shape 66
7.4.2 Plane Projection 70
7.5 Dynamical Simulations **72**

8 DISCUSSION **79**
8.1 Centroid of the GC Distribution **79**
8.2 Effects of Small Sample Size **80**
8.3 Structures **80**

9 CONCLUSIONS **85**

BIBLIOGRAPHY **87**

1 Introduction

Globular Clusters (GCs) are tightly bound groups of thousands, and sometimes millions, of stars. Along formation and billions of years of evolution, they possess a higher stellar density than open clusters and are fossils that keep information about primordial eras. Some of the brightest GCs, such as ω Centauri, have been observed throughout the centuries, long before the development of astrophysics as we know today. Our understanding of their structure has evolved alongside several fields of study, from optics to quantum mechanics, but they still hold perplexing features which are not fully explained yet.

1.1 Historical Background

> "ω Centauri (Bode) is a beautiful large bright round nebula, about 10' or 12' diameter, easily resolvable to the very centre; it is a beautiful globe of stars very gradually and moderately compressed to the centre; the stars are rather scattered preceding and following, and the greatest condensation is rather north of the centre: the stars are of slightly mixed magnitudes, or a white colour. This is the largest bright nebula in the southern hemisphere." (Dunlop, 1828, p. 136)

In the past, any diffuse astronomical object, from star clusters to galaxies, were simply called *nebulae*. With the advent of telescopes powerful enough to resolve individual stars, the classification of non-stellar objects became increasingly complex. The term *globular cluster* can already be found in William Herschel's *Catalogue of a Second Thousand of New Nebulae and Clusters of Stars*, first published in 1789, defined as a "spherically shaped" structure (Herschel, 1789, p. 214).

Shapley (1916), and subsequent papers, is one of the earliest studies about star clusters. Shapley admits the various proposed classifications still relied on loosely defined, arbitrary characteristics, and suggests the usage of the cluster's central density as the defining parameter that separates open from globular clusters. According to him, this allows a sharp discrimination between the two kinds of

object. Representations of stellar distribution had been suggested at least since 1908, by Hugo von Zeipel, but it would take over 50 years until Ivan R. King's semi-theoretical functions were introduced (Hanes; Madore, 1980, p. 5).

Visual photometers, as well as bandpass filters, have been used since the middle of the 19th century, giving room to the creation of different photometric systems and magnitude scales [1]. By 1911, the earliest version of the Hertzsprung-Russel (H-R) diagram was published (Hertzsprung, 1911). In 1915, Harlow Shapley noted that stars belonging to GCs seemed to concentrate in a narrow region of the H-R diagram (Hanes; Madore, 1980, p. 4). A breakthrough was made by Baade (1944), who identified a sharp difference in the H-R diagrams of the solar neighbourhood and those of GCs: the presence of a horizontal branch (HB) and a bright red giant branch (RGB). Their features in the H-R diagram or, similarly, in a color-magnitude diagram (CMD), are strong indicators that separate them from open clusters and field stars.

Spectrographs were already being aimed at distant stars during the earliest years of the 20th century. In the past thirty years, several chemical peculiarities were detected in GCs. Of particular importance is the sharp difference in the $[Na/O]$ abundance between GC stars and similar field stars (Gratton; Sneden; Carretta, 2004, and references therein). These two elements are invariably anticorrelated in GCs, making this feature a powerful tool to categorize them as such.

With the number of objects in this star cluster category, it is relevant to study them as a population. Sawyer (1949) published one of the earliest Galactic GC catalogues, a work of over twenty years, with 99 objects. The work of Webbink (1985) presented observational and structural parameters for 154 GCs and candidates. Presently, the most widely used catalogue is the 2010 edition of Harris (1996), with data for 157 GCs. As vastly better observational estimates became available with CCDs (charge-coupled devices), the focus of catalogues had to shift from only adding objects to updating parameters of known ones.

A sample of Galactic GCs is fundamental to the study of the evolution of the Milky Way, and GC catalogues are essential for this undertaking. It is not trivial,

[1] For more information, see Miles (2007), *"A light history of photometry: from Hipparchus to the Hubble Space Telescope"*.

however, to produce a "pure" GC sample, without open clusters or extragalactic objects (Sect. 2.1). GCs have been used as clues in Galactic archeology since our first insights into their nature (Sect. 1.2). Knowing they are old, with ages typically greater than 10 Gyr, we can infer that they hold primordial information about their host galaxies. The most fundamental question pertains their very formation - how do galaxies come to be? An assortment of models have been proposed, a few of which directly connected to GCs (Hanes; Madore, 1980, p. 175).

Early models assume a scenario where a massive and approximately spherical gas cloud undergoes a dissipative and monolithic collapse, with characteristics like a free-fall regime and low metallicity (Eggen; Lynden-Bell; Sandage, 1962). It is possible to infer from such event that the GC distribution will be symmetrical in several parameters, both spatial and structural. The clusters would necessarily be native to their host galaxies, all originating from the same primordial cloud. The monolithic collapse model was later reformulated to include chemical enrichment to explain the wide range of observed metallicities. More recent models take into account that other processes were important for the Galaxy to present the characteristics that we now observe: interactions with or even complete accretions of neighbouring galaxies, a mechanism named hierarchical accretion of satellites. Such events could have happened on both remote (Searle; Zinn, 1978, Zinn, 1980) and recent eras (Ibata; Gilmore; Irwin, 1994, Ibata et al., 1997). Accreted satellites may have left behind clues of their existence, such as their nuclei, streams, or even their GCs.

As early as 1978, it was suggested that the young Magellanic Cloud globular clusters might have been created in interactions with the Milky Way (Hanes; Madore, 1980, p. 307). Could some of our Galactic GCs have arisen from similar events? Or even more drastically - could they be entirely external objects that were accreted? Two Milky Way GCs known to be relatively young were probed by Lin & Richer (1992): Palomar 12 and Ruprecht 106, which appeared to be 3 Gyrs and $4-5$ Gyrs younger than similar clusters, respectively. The authors constructed a family of orbits consistent with a tidal capture scenario that removed them from the Magellanic Clouds, however they admit that the evidence for Palomar 12 is somewhat weaker. Few years later, with more precise absolute proper

motion measurements, Dinescu et al. (2000) conclude that it is more likely that the Magellanic Clouds were not Palomar 12's origin, but rather the Sagittarius Dwarf Spheroidal. Palomar 12 and Ruprecht 106 are also unique in regards to chemical abundances, presenting a deficiency in all α elements unseen in any other GC (Gratton; Sneden; Carretta, 2004).

The core of the Sagittarius galaxy, also known as Messier 54 or NGC 6715, was discovered by Charles Messier in 1778, and later confirmed to be a tidally-disrupted dwarf galaxy (Ibata; Gilmore; Irwin, 1994). Lynden-Bell & Lynden-Bell (1995) proposed that GCs dragged in tidal debris into the Galaxy would delinate the infall orbit of their accreted host, and proceeded to search for other surviving members of the Sagittarius galaxy currently being torn apart by the Milky Way. They predicted that Palomar 2, Arp 2, and probably Terzan 7 might be related to the Sagittarius galaxy. Since then, the list of candidates was expanded to include NGC 4147, Terzan 8, Palomar 12, and Whiting 1 (van den Bergh, 2007, and references therein). With our ability to detect ever smaller and fainter objects, differentiating GCs from not only open clusters but also dwarf galaxies becomes relevant as well. A popular criterion is the object's position in a surface luminosity versus size plot.

The Sagittarius system, notorious as it is, remains the single strong and widely accepted evidence of galactic cannibalism in the Milky Way. The nature of other candidate, the Canis Major Overdensity, is still under debate. Regardless of whether the overdensity is a disk warp or a dwarf galaxy, Martin et al. (2004) found that four GCs surround the structure with compatible radial velocity, alongside a number of open clusters. Their work followed previous simulations which show that the thin and thick disk of a Milky Way-like galaxy do not share a common origin, with the latter being constructed mainly through in-plane accretions. They concluded that, within the limitations of their model, the simulations of a Milky Way-like galaxy in this accretion scenario resulted in a structure similar to the observed Canis Major Overdensity. However, this is still disputed.

GCs can also be found in the centre of a cosmological debate. It has been known since Lynden-Bell (1976) that the 11 classical satellite dwarf galaxies of the Milky Way seemed to be distributed in a preferential plane, a large circle

almost perpendicular to the Galactic disk. This structure is known, among other denominations, as the Vast Polar Structure (VPoS). By the early 2000s, 13 newly detected dwarf galaxies (DGALs) also seemed to be contained in it (York et al., 2000). Pawlowski, Pflamm-Altenburg & Kroupa (2012) for the first time studied how known streams and GCs were positioned in relation to the VPoS, offering strong, albeit debated, arguments against the λ-CDM model.

Going back to what is maybe the most fundamental structure astrophysics concerns itself with, GCs have also been in the spotlight in the study of stellar evolution. GCs have long been known to hold a host of unusual objects like O and B-type subdwarfs, millisecond pulsars, blue stragglers and an assortmnent of variables. The existence of such special stars could be attributed to their long age and dynamical interactions, and their study was vital to our understanding of stellar evolution. As for the "typical" stars, the observed GC CMDs, with a large number of objects, give firm constraints to theoretical isochrones, which in turn rely on the complex computation of the physical mechanisms within stars. In the past, the formation of GCs was believed to be a type of monolithic collapse as well, making mass the only difference between the stars of a given GC. Age and metallicity would be, in turn, the difference between two GCs. With the lower resolution photometry of past decades, it was reasonable to assume that a single isochrone could fit an observed CMD, with any inconsistencies being due to uncertainties.

However, chemical abundance variations in "common" stars could be detected in the early 1970s, introducing a challenge to the simple population model. Wayne Osborn observed, in 1971, one star in M5 and another in M10 that showed considerable difference in the CN bands when compared to the rest of their respective clusters (Osborn, 1971). Cohen (1978) observed a considerable scatter for Na and Ca in M3, with Ca being one of the two easily observed elements produced exclusively via alpha-process. In the following years, it was established that globular clusters were indeed very heterogenous not only in C and N, but several observationally accessible light elements (Li, O, Na, Mg, and Al). A spread in Fe and heavier elements was, however, restricted to the more massive clusters, such as ω Centauri.

The higher resolution of modern equipment brought a radical paradigm shift. The first clear photometric evidence of multiple stellar populations was found in ω Centauri (Bedin et al., 2004), in the form of two clearly distinct lower main sequences whereas in past decades only a wide giant branch could be detected (Cannon; Stobie, 1973). Piotto et al. (2005) analysed the spectra of those two populations, concluding that an He enrichment could explain their differences. The same hypothesis could also explain the three MSs observed in NGC 2808 (D'Antona et al., 2005): Piotto et al. (2007) showed that three populations with the same age and metallicity but three different He abundances could create the observed CMD. Since then, several cases of multiple populations have been observed photometrically.

In light of these discoveries, it became necessary to determine how those multiple populations could have formed. Were some of them caused by chemical inhomogenities in the primordial gas cloud that gave origin to the cluster? Could they be explained by dynamical interactions, mixing mechanisms or self-enrichment? Was there a large missing piece of our stellar evolution models? Bastian (2015) concluded that of the several scenarios that had been put forward, none of them could explain the observations.

Further study of GCs, if the many past decades behind us are any clue, will bring forth the answers, and perhaps even more questions. With their extremely long lifetime, GCs are witnesses to galactic formation itself. Their attributes like metallicity and spatial distribution serve as powerful evidence to support or discard different galactic formation model. These fascinating objects display a complex structure that provides constraints on multiple fields of astrophysics. From the modeling of stellar evolution to theories of how the Milky Way came to be, the investigation of GCs remains essential.

1.2 The Present Work

GCs are an elementary component of the Galaxy, and their centroids may or may not coincide. The distance to the Galactic centre (R_0) is fundamental in several fields of astronomy and astrophysics. Models of mass and luminosity of

objects inside the Galaxy, calibration of extragalactic distances, ages of stars and clusters, and even the Hubble Constant (and consequently the rate of acceleration of the universe) are dependent on R_0 (Reid, 1993).

In 1918 and with a sample of 69 GCs, Harlow Shapley estimated their distances to the Sun and inferred their positions in a face-on view of the Milky Way (Shapley, 1918). It was evident that the clusters were heavily concentrated towards Sagittarius and not at all symmetrically distributed around us. Shapley suggested that their symmetrical point was the Galactic centre, which laid at an estimated distance of $R_0 = 13$ kpc from the Sun. Back then, interestellar extinction was completely unknown, so the GC distances were overestimated. The idea that the Milky Way was just one of many spiral galaxies was still in its infancy, and GCs were offering a distance scale that would eventually make it evident that many observed objects were actually external to the Galaxy. The technique pioneered by Shapley has been reproduced many times since his initial work, with an increasing number of GCs and better estimates of their distances (Reid, 1993).

Keeping in mind the importance of R_0, it is no surprise that its value has been the subject of intense debate for over a century. Current research points to a relatively small range of values: 7 to 8.5 kpc. Reid (1993) presented a deep revision of the several methods employed in the determination of R_0, their limitations and theoretical constraints, and also evidence of a bias for values found from 1974 to the 1990s (Foster; Cooper, 2010). A similar work was made by Turner (2014), showing both recent values of R_0 and their respective methods of acquisition, including a value found by his own work that considers the orbit of the Sun, $R_0 = 8.4 \pm 0.27$ kpc. This possible bias was also discussed by Malkin (2013), this time being called bandwagon effect. Reviewing 52 values of R_0 from the last twenty years, he concluded that there currently is no significant bias, though perhaps there was in past decades, and that the errors have been systematically decreasing. His data point to a mean value of $R_0 = 7.97$ kpc, with a maximum of 8.8 kpc and a minimum of 7.0 kpc. Foster & Cooper (2010) found $R_0 = 8.4$ kpc as a mean value. More recently, the centre has been estimated with VVV (VISTA Variables in the Via Lactea) using RR Lyrae to be 8.33 ± 0.14 kpc (Dékány et al., 2013). Estimation methods that use GCs seem to consistently point at smaller values. (Bica et al.,

2006) (hereafter B06) found $R_0 = 7.2 \pm 0.3$ kpc, while Francis & Anderson (2014) found $R_0 = 7.4 \pm 0.2|_{stat} \pm 0.2|_{sys}$ kpc.

One of our objectives in the present work is to find the centroid of the GC distribution and infer how it relates to R_0. As GCs are old objects that might predate the disk, it is reasonable to assume they mostly populate the halo, specially with the high destruction rate due to bulge-shocking (Aguilar; Hut; Ostriker, 1988, Moreno; Pichardo; Velázquez, 2014) or disk-crossing (Odenkirchen et al., 2009). Therefore, discoveries of GCs in the central regions of the Galaxy are of particular interest because of their proximity to structures like the spiral arms and the bar. Their survival in these turbulent regions suggests that their orbits could be significantly altered by interactions with the bulge, bar, and disk, perhaps even forming detectable structures, a possibility we will investigate in the present work. Detection of such structures would be strongly dependent on distance uncertainties and the dynamics of orbits, which we will investigate as well.

1.3 Objectives

In this study, we estimate the distance between the Sun and the centre of the Galactic GC spatial distribution, with updated data and new methods. We group GCs with similar characteristics such as metallicity and study the effect they have on the general distribution. Additionally, we seek to identify asymmetries in the spatial distribution of GCs and their relationship to known structures in the Milky Way. We apply statistical methods to evaluate the significance of these asymmetries and how they are affected by possible over- or underestimations of GC distance uncertainties. Finally, we use an axisymmetric potential to estimate orbits for GCs with available proper motions and radial velocities to determine if any asymmetries are transient.

In Sect. 2, we discuss the difficulties on defining a univocal GC sample and present the data, including new objects found in the last six years [2]. A brief analysis of known dust clouds and how they relate to known GC positions is presented

[2] A GC candidate, Kim 3, has been recently discovered and was not included in this study. The star cluster is the least luminous known to date, with an age of $9.5^{+3.0}_{-1.7}$ Gyr, and appears to be in the final stages of tidal disruption (Kim et al., 2016).

in Sect. 3. In Sect. 4, we present the results of our analysis on determining the distance uncertainties of GCs. Subsamples for the GCs according to characteristics in common are derived in Sect. 5. Methods are discussed in Sect. 6. Results are presented in Sect. 7 and discussed in Sect. 8. Finally, we present conclusions and perspectives in Sect. 9.

2 Data

2.1 Defining a Globular Cluster Catalogue

Several studies in recent years have provided observational constraints that shape attempts to compile a general GC catalogue. Some GCs in the 2010 edition of Harris (1996) (hereafter H10) have been further studied. BH 176 was classified as an old open cluster (Davoust; Sharina; Donzelli, 2011), and so was GLIMPSE-C01 (Davies et al., 2011). Therefore, uncertainties or ambiguous classifications exist for part of the objects especially at low Galactic latitudes. At high b values, other classifications have been proposed. Koposov 1 and 2 appear to be open clusters that were torn off from the Sagittarius Dwarf, having relatively young ages of 7 and 5 Gyr, respectively (Paust; Wilson; van Belle, 2014).

In the Milky Way, GCs are expected to be old stellar systems, typically with ages $\geq$ 10 Gyr (B06). The latter study reported 19 relatively young GCs, with Palomar 1 as young as $6-8$ Gyr, thus younger than several old open clusters (Ortolani et al., 2005). Some GCs appear to be stripped dwarf galaxy nuclei. M54 (NGC 6715) is undoubtedly the nucleus of the Sagittarius Dwarf, while ω Centauri and NGC 2419 and are probably stripped ones (B06 and references therein).

Current studies point to specific chemical characteristics that can aid in the unambiguous categorization of star clusters (Gratton; Sneden; Carretta, 2004). Open clusters, field stars and GCs all present similar values of $[Ni/Fe]$, with the exception of Palomar 12 and Ruprecht 106, which present other chemical anomalies which might point to an extragalactic origin. All GCs present an anticorrelation between Na and O in their evolved RGB stars, a feature not present in similar field stars. The study of chemical abundances might be the key to building a definitive Galactic GC sample and identifying GC with atypical formation histories.

Some clusters present structural features such as a tidal tail and might be dissolving, e.g. the low mass Palomar 5 (Odenkirchen et al., 2009). The massive GC NGC 1851 presents an unusual halo beyond the tidal radius (Marino et al.,

2014). Thus not all GCs share a standard structure and many possess unusual characteristics. Multiple stellar populations are to date a major issue about GCs, and they are being systematically tested on growing samples of GCs. Those with two stellar populations appear to be the rule (Gratton; Carretta; Bragaglia, 2012). However as many as four (Villanova et al., 2007, ω Centauri), and five (Milone et al., 2015, NGC 2808) have been observed. Simple populations have been observed so far only in 2 GCs, namely Ruprecht 106 (Villanova et al., 2013) and E3 (Salinas; Strader, 2015).

Can a GC catalogue be uniquely defined with our current knowledge? All the above objects are in H10, but rather than pruning this reference catalogue, we decided to (i) keep the whole previous sample, (ii) update it with the objects presented in Tab. 1, and (iii) follow B06 to use labels in Tab. 2 to characterize the objects according to their special features (e.g. young, associated galaxy nucleus, association to dwarfs or streams).

2.2 The Sample

The full sample was collected from H10, with 157 objects. We added new GCs, increasing their number to 170 (Tab. 1). With this approach, we compiled reddening values, metallicities, and distances.

We included objects in different parts of the Galaxy. FSR 1767 and Kronberger 49 are in crowded fields, and are probable globular clusters. Until recently, Mercer 5 was in a similar situation (Longmore et al., 2011), but has been confirmed as a GC (Peñaloza et al., 2015). There are GC candidates in the VVV Survey that require further probing. We cite VVV CL001 (Minniti et al., 2011), VVV CL003 and VVV CL004 (Moni Bidin et al., 2011), and several more (Bica; Ortolani; Barbuy, 2016). Most of the newly added halo GCs are in the outer parts and are confirmed as such. One can find both old and extremely young (e.g. Muñoz 1 with 12.5 Gyr, and Segue 3 with 3.2 Gyr, references in Tab. 1). The case of Segue 3 is particularly interesting as Galactic GCs are typically older than $10Gyr$, so even with ages around $8Gyr$ such objects could be considered young.

We have also updated six clusters with more recent data: Terzan 10

Table 1 – Additions to H10 and their corresponding discovery and/or analysis papers.

Name	Reference	Comments
Balbinot 1	Balbinot et al. (2013)	Halo
DES 1	Luque et al. (2016)	Halo
FSR 1767	Bonatto et al. (2009)	Bulge?
Kim 1	Kim & Jerjen (2015)	Halo
Kim 2	Kim et al. (2015)	Halo
Kronberger 49	Ortolani et al. (2012)	Bulge
Laevens 1 (Crater)	Laevens et al. (2014), Kirby, Simon & Cohen (2015)	Halo
Laevens 3	Laevens et al. (2015)	Halo
Mercer 5	Peñaloza et al. (2015)	Bulge
Muñoz 1	Muñoz et al. (2012)	Halo
Pfleiderer 2	Ortolani et al. (2009)	Halo
Segue 3	Ortolani, Bica & Barbuy (2013)	Halo
VVV CL002	Moni Bidin et al. (2011)	Bulge

and 2MASS GC02 (Alonso-García et al., 2015), GLIMPSE-C01 (Ivanov; Kurtev; Borissova, 2005), Koposov 1 and Koposov 2 (Paust; Wilson; van Belle, 2014), and UKS 1 (Ortolani et al. in preparation). Galactic coordinates, distances from the Sun, absolute magnitudes, metallicities, color excesses, and group classification are given in Tab. 2 for the 170 GCs. The group classification is explained on Sect. 5. Proper motions and radial velocities are given in Tab. 3 for 68 GCs.

Information about proper motions and radial velocities (Tab. 3) were extracted from Dinescu, Girard & van Altena (1999), Dinescu et al. (2003), Casetti-Dinescu et al. (2007), Casetti-Dinescu et al. (2013), Casetti-Dinescu et al. (2010), Pryor, Piatek & Olszewski (2010), Siegel et al. (2001), Milone et al. (2006), Kalirai et al. (2007), and Rossi et al. (2015). In cases where the same object was present in multiple works, the most recently published data was adopted.

Table 2 – The GC sample.

Name	$l_{(deg)}$	$b_{(deg)}$	$R_{\odot}$	M_V	$[Fe/H]$	$E(B\text{-}V)$	Groups
2MASS GC01	10.471	0.100	3.6	−6.11		6.80	
2MASS GC02	9.782	−0.615	7.1	−4.86	−1.08	5.16	
47 Tucanae (NGC 104)	305.895	−44.889	4.5	−9.42	−0.72	0.04	O
AL 3 (BH 261)	3.362	−5.270	6.5	−4.19	−1.30	0.36	
AM 1 (E 1)	258.361	−48.471	123.3	−4.73	−1.70	0.00	
AM 4	320.284	33.507	32.2	−1.81	−1.30	0.05	
Arp 2	8.545	−20.785	28.6	−5.29	−1.75	0.10	S, Y
Balbinot 1	75.180	−32.638	31.9	−1.21	−1.58	0.06	
BH 176	328.413	4.337	18.9	−4.06	0.00	0.54	Y
DES 1	310.523	−67.831	87.1	−3.05	−1.98	0.00	
Djorg 1	356.675	−2.482	13.7	−6.98	−1.51	1.58	
E 3	292.268	−19.017	8.1	−4.12	−0.83	0.30	O
Eridanus	218.106	−41.332	90.1	−5.13	−1.43	0.02	Y
ESO280-SC06	346.899	−12.571	21.4	−4.87	−1.80	0.07	
ESO452-SC11	351.911	12.097	8.3	−4.02	−1.50	0.46	
ESO456-SC38 (Djorg 2)	2.764	−2.508	6.3	−7.00	−0.65	0.94	
FSR 1735	339.188	−1.853	9.8	−6.45		1.42	
FSR 1767	352.600	−2.173	1.5	−4.7	−1.00	2.00	
GLIMPSE-C01	31.302	−0.102	3.7	−5.91	−1.61	4.85	

Continues on next page ...

Continued from previous page.

Name	$l_{(deg)}$	$b_{(deg)}$	$R_{\odot}$	M_V	$[Fe/H]$	$E(B\text{-}V)$	Groups
GLIMPSE-C02	14.128	−0.645	5.5		−0.33	7.85	
HP 1 (BH 229)	357.425	2.115	8.2	−6.46	−1.00	1.12	
IC 1257	16.528	15.145	25.0	−6.15	−1.70	0.73	
IC 1276 (Pal 7)	21.832	5.669	5.4	−6.67	−0.75	1.08	
IC 4499	307.354	−20.473	18.8	−7.32	−1.53	0.23	Y
Kim 1	68.515	−38.426	19.8	0.3	−1.70	0.11	
Kim 2	347.159	−42.074	104.7	−1.5	−1.00	0.03	
Koposov 1	260.975	70.754	34.9	−1.35	−0.60	0.01	Y
Koposov 2	196.156	25.214	33.3	−0.35	−0.60	0.08	Y
Kronberger 49	7.627	−2.012	8.0	−5.1	−0.10	1.35	
Laevens 1 (Crater)	274.810	47.850	145.0	−4.3	−1.68	0.03	
Laevens 3	63.592	−21.175	67.0	−4.4	−1.90	0.07	
Liller 1	354.841	−0.160	8.2	−7.32	−0.33	3.07	
Lynga 7 (BH 184)	328.769	−2.797	8.0	−6.60	−1.01	0.73	O
Mercer 5	17.594	−0.109	5.5		−0.86	− − −	
Muñoz 1	105.441	45.480	45.0	−0.4	−1.50	0.02	
NGC 1261	270.539	−52.124	16.3	−7.80	−1.27	0.01	Y
NGC 1851	244.513	−35.036	12.1	−8.33	−1.18	0.02	Y, C, R
NGC 1904 (M 79)	227.230	−29.350	12.9	−7.86	−1.60	0.01	C
NGC 2298	245.629	−16.006	10.8	−6.31	−1.92	0.14	C, O

Continues on next page ...

Continued from previous page.

Name	$l_{(deg)}$	$b_{(deg)}$	$R_{\odot}$	M_V	$[Fe/H]$	$E(B\text{-}V)$	Groups
NGC 2419	180.369	25.242	82.6	−9.42	−2.15	0.08	DN
NGC 2808	282.193	−11.253	9.6	−9.39	−1.14	0.22	C, Y
NGC 288	151.285	−89.380	8.9	−6.75	−1.32	0.03	R, Y
NGC 3201	277.229	8.640	4.9	−7.45	−1.59	0.24	R, Y
NGC 362	301.533	−46.247	8.6	−8.43	−1.26	0.05	Y, R
NGC 4147	252.848	77.189	19.3	−6.17	−1.80	0.02	R, ST, Y
NGC 4372	300.993	−9.884	5.8	−7.79	−2.17	0.39	
NGC 4590 (M 68)	299.626	36.051	10.3	−7.37	−2.23	0.05	O
NGC 4833	303.604	−8.015	6.6	−8.17	−1.85	0.32	O
NGC 5024 (M 53)	332.963	79.764	17.9	−8.71	−2.10	0.02	O
NGC 5053	335.699	78.946	17.4	−6.76	−2.27	0.01	O
ω Centauri (NGC 5139)	309.102	14.968	5.2	−10.26	−1.53	0.12	DN, R, Y
NGC 5272 (M 3)	42.217	78.707	10.2	−8.88	−1.50	0.01	Y
NGC 5286	311.614	10.568	11.7	−8.74	−1.69	0.24	CT, O
NGC 5466	42.150	73.592	16.0	−6.98	−1.98	0.00	O
NGC 5634	342.209	49.260	25.2	−7.69	−1.88	0.05	
NGC 5694	331.056	30.360	35.0	−7.83	−1.98	0.09	
NGC 5824	332.555	22.070	32.1	−8.85	−1.91	0.13	DN
NGC 5897	342.946	30.294	12.5	−7.23	−1.90	0.09	
NGC 5904 (M 5)	3.859	46.796	7.5	−8.81	−1.29	0.03	Y

Continues on next page ...

Continued from previous page.

Name	$l_{(deg)}$	$b_{(deg)}$	$R_{\odot}$	M_V	$[Fe/H]$	$E(B\text{-}V)$	Groups
NGC 5927	326.604	4.860	7.7	−7.81	−0.49	0.45	O
NGC 5946	327.583	4.191	10.6	−7.18	−1.29	0.54	
NGC 5986	337.022	13.268	10.4	−8.44	−1.59	0.28	O
NGC 6093 (M 80)	352.673	19.463	10.0	−8.23	−1.75	0.18	O
NGC 6101	317.746	−15.825	15.4	−6.94	−1.98	0.05	O
NGC 6121 (M 4)	350.973	15.972	2.2	−7.19	−1.16	0.35	O
NGC 6139	342.366	6.939	10.1	−8.36	−1.65	0.75	
NGC 6144	351.929	15.701	8.9	−6.85	−1.76	0.36	O
NGC 6171 (M 107)	3.373	23.011	6.4	−7.12	−1.02	0.33	O
NGC 6205 (M 13)	59.007	40.913	7.1	−8.55	−1.53	0.02	R, Y
NGC 6218 (M 12)	15.715	26.313	4.8	−7.31	−1.37	0.19	O
NGC 6229	73.639	40.307	30.5	−8.06	−1.47	0.01	
NGC 6235	358.918	13.518	11.5	−6.29	−1.28	0.31	
NGC 6254 (M 10)	15.137	23.076	4.4	−7.48	−1.56	0.28	Y
NGC 6256	347.792	3.307	10.3	−7.15	−1.02	1.09	
NGC 6266 (M 62)	353.574	7.318	6.8	−9.18	−1.18	0.47	
NGC 6273 (M 19)	356.869	9.382	8.8	−9.13	−1.74	0.38	
NGC 6284	358.346	9.940	15.3	−7.96	−1.26	0.28	
NGC 6287	0.131	11.024	9.4	−7.36	−2.10	0.60	
NGC 6293	357.620	7.834	9.5	−7.78	−1.99	0.36	

Continues on next page ...

Continued from previous page.

Name	$l_{(deg)}$	$b_{(deg)}$	$R_{\odot}$	M_V	$[Fe/H]$	$E(B\text{-}V)$	Groups
NGC 6304	355.826	5.376	5.9	−7.30	−0.45	0.54	O
NGC 6316	357.175	5.764	10.4	−8.34	−0.45	0.54	
NGC 6325	0.973	8.004	7.8	−6.96	−1.25	0.91	
NGC 6333 (M 9)	5.544	10.707	7.9	−7.95	−1.77	0.38	
NGC 6341 (M 92)	68.338	34.859	8.3	−8.21	−2.31	0.02	O
NGC 6342	4.899	9.725	8.5	−6.42	−0.55	0.46	
NGC 6352	341.421	−7.166	5.6	−6.47	−0.64	0.22	O
NGC 6355	359.585	5.428	9.2	−8.07	−1.37	0.77	
NGC 6356	6.724	10.220	15.1	−8.51	−0.40	0.28	
NGC 6362	325.555	−17.570	7.6	−6.95	−0.99	0.09	O
NGC 6366	18.409	16.036	3.5	−5.74	−0.59	0.71	O
NGC 6380 (Tonantzintla 1)	350.181	−3.420	10.9	−7.50	−0.75	1.17	
NGC 6388	345.556	−6.738	9.9	−9.41	−0.55	0.37	O
NGC 6397	338.165	−11.960	2.3	−6.64	−2.02	0.18	O
NGC 6401	3.451	3.980	10.6	−7.90	−1.02	0.72	
NGC 6402 (M 14)	21.324	14.805	9.3	−9.10	−1.28	0.60	
NGC 6426	28.087	16.234	20.6	−6.67	−2.15	0.36	
NGC 6440	7.729	3.801	8.5	−8.75	−0.36	1.07	
NGC 6441	353.532	−5.006	11.6	−9.63	−0.46	0.47	O
NGC 6453	355.717	−3.872	11.6	−7.22	−1.50	0.64	

Continues on next page ...

Continued from previous page.

Name	$l_{(deg)}$	$b_{(deg)}$	$R_{\odot}$	M_V	$[Fe/H]$	$E(B\text{-}V)$	Groups
NGC 6496	348.027	−10.014	11.3	−7.20	−0.46	0.15	O
NGC 6517	19.225	6.763	10.6	−8.25	−1.23	1.08	
NGC 6522	1.025	−3.925	7.7	−7.65	−1.34	0.48	
NGC 6528	1.138	−4.174	7.9	−6.57	−0.11	0.54	
NGC 6535	27.176	10.436	6.8	−4.75	−1.79	0.34	Y
NGC 6539	20.795	6.776	7.8	−8.29	−0.63	1.02	
NGC 6540 (Djorg 3)	3.285	−3.313	5.3	−6.35	−1.35	0.66	
NGC 6541	349.286	−11.188	7.5	−8.52	−1.81	0.14	O
NGC 6544	5.838	−2.204	3.0	−6.94	−1.40	0.76	
NGC 6553	5.253	−3.030	6.0	−7.77	−0.18	0.63	
NGC 6558	0.199	−6.023	7.4	−6.44	−1.32	0.44	
NGC 6569	0.481	−6.681	10.9	−8.28	−0.76	0.53	
NGC 6584	342.143	−16.414	13.5	−7.69	−1.50	0.10	Y
NGC 6624	2.788	−7.913	7.9	−7.49	−0.44	0.28	O
NGC 6626 (M 28)	7.798	−5.580	5.5	−8.16	−1.32	0.40	
NGC 6637 (M 69)	1.723	−10.269	8.8	−7.64	−0.64	0.18	O
NGC 6638	7.897	−7.153	9.4	−7.12	−0.95	0.41	
NGC 6642	9.815	−6.439	8.1	−6.66	−1.26	0.40	
NGC 6652	1.534	−11.377	10.0	−6.66	−0.81	0.09	O
NGC 6656 (M 22)	9.892	−7.552	3.2	−8.50	−1.70	0.34	O

Continues on next page ...

Continued from previous page.

Name	$l_{(deg)}$	$b_{(deg)}$	$R_{\odot}$	M_V	$[Fe/H]$	$E(B\text{-}V)$	Groups
NGC 6681 (M 70)	2.853	−12.510	9.0	−7.12	−1.62	0.07	O
NGC 6712	25.354	−4.318	6.9	−7.50	−1.02	0.45	
NGC 6715 (M 54)	5.607	−14.087	26.5	−9.98	−1.49	0.15	S, DN, Y
NGC 6717 (Palomar 9)	12.876	−10.900	7.1	−5.66	−1.26	0.22	O
NGC 6723	0.069	−17.299	8.7	−7.83	−1.10	0.05	O
NGC 6749	36.201	−2.205	7.9	−6.70	−1.60	1.50	
NGC 6752	336.493	−25.628	4.0	−7.73	−1.54	0.04	Y
NGC 6760	36.108	−3.924	7.4	−7.84	−0.40	0.77	
NGC 6779 (M 56)	62.659	8.336	9.4	−7.41	−1.98	0.26	R, O
NGC 6809 (M 55)	8.793	−23.272	5.4	−7.57	−1.94	0.08	O
NGC 6838 (M 71)	56.746	−4.564	4.0	−5.61	−0.78	0.25	O
NGC 6864 (M 75)	20.304	−25.747	20.9	−8.57	−1.29	0.16	R
NGC 6934	52.103	−18.893	15.6	−7.45	−1.47	0.10	R, Y
NGC 6981 (M 72)	35.162	−32.683	17.0	−7.04	−1.42	0.05	R, Y
NGC 7006	63.769	−19.407	41.2	−7.67	−1.52	0.05	R
NGC 7078 (M 15)	65.013	−27.313	10.4	−9.19	−2.37	0.10	O
NGC 7089 (M 2)	53.371	−35.770	11.5	−9.03	−1.65	0.06	Y
NGC 7099 (M 30)	27.179	−46.836	8.1	−7.45	−2.27	0.03	R, O
NGC 7492	53.386	−63.477	26.3	−5.81	−1.78	0.00	R
Palomar 1	130.065	19.028	11.1	−2.52	−0.65	0.15	Y, CT

Continues on next page ...

Continued from previous page.

Name	$l_{(deg)}$	$b_{(deg)}$	$R_{\odot}$	M_V	$[Fe/H]$	$E(B\text{-}V)$	Groups
Palomar 10	52.436	2.725	5.9	−5.79	−0.10	1.66	
Palomar 11	31.805	−15.576	13.4	−6.92	−0.40	0.35	
Palomar 12	30.510	−47.682	19.0	−4.47	−0.85	0.02	Y, ST
Palomar 13	87.104	−42.700	26.0	−3.76	−1.88	0.05	R
Palomar 14 (AvdB)	28.746	42.192	76.5	−4.80	−1.62	0.04	
Palomar 15	18.849	24.337	45.1	−5.51	−2.07	0.40	
Palomar 2	170.530	−9.072	27.2	−7.97	−1.42	1.24	
Palomar 3	240.141	41.865	92.5	−5.69	−1.63	0.04	Y
Palomar 4	202.311	71.803	108.7	−6.01	−1.41	0.01	Y
Palomar 5	0.852	45.860	23.2	−5.17	−1.41	0.03	Y
Palomar 6	2.092	1.780	5.8	−6.79	−0.91	1.46	
Palomar 8	14.105	−6.797	12.8	−5.51	−0.37	0.32	
Pfleiderer 2	22.281	9.322	16.0	−2.5	0.00	1.01	
Pyxis	261.319	6.997	39.4	−5.73	−1.20	0.21	
Ruprecht 106	300.888	11.671	21.2	−6.35	−1.68	0.20	Y
Segue 3	69.399	−21.272	29.1	−1.2	−0.80	0.09	
Terzan 1 (HP 2)	357.569	0.996	6.7	−4.41	−1.03	1.99	
Terzan 10	4.420	−1.890	10.3	−6.35	−1.00	2.40	
Terzan 12	8.358	−2.101	4.8	−4.14	−0.50	2.06	
Terzan 2 (HP 3)	356.319	2.298	7.5	−5.88	−0.69	1.87	

Continues on next page ...

Continued from previous page.

Name	$l_{(deg)}$	$b_{(deg)}$	$R_{\odot}$	M_V	$[Fe/H]$	$E(B\text{-}V)$	Groups
Terzan 3	345.076	9.187	8.2	−4.82	−0.74	0.73	
Terzan 4 (HP 4)	356.024	1.308	7.2	−4.48	−1.41	2.00	
Terzan 5 (Terzan 11)	3.839	1.687	6.9	−7.42	−0.23	2.28	
Terzan 6 (HP 5)	358.571	−2.162	6.8	−7.59	−0.56	2.35	
Terzan 7	3.387	−20.067	22.8	−5.01	−0.32	0.07	S, Y
Terzan 8	5.759	−24.559	26.3	−5.07	−2.16	0.12	S, O
Terzan 9	3.603	−1.989	7.1	−3.71	−1.05	1.76	
Tonantzintla 2 (Pismis 26)	350.796	−3.423	8.2	−6.17	−0.70	1.24	
UKS 1	5.125	0.764	14.6	−6.91	−0.70	3.14	
VVV CL002	359.559	0.889	7.3	−3.4	−0.40	2.88	
Whiting 1	161.618	−60.636	30.1	−2.46	−0.70	0.03	Y

Table 3 – Proper motions and radial velocities.

Name	$\mu_{\alpha cos(\delta)}$ (mas yr^{-1})	μ_{δ} (mas yr^{-1})	$R_{\odot}$ kpc	V_{rad} (km s^{-1})
47 Tucanae (NGC 104)	5.61 ± 0.96	-3.40 ± 0.93	4.30	-18.70 ± 0.20
NGC 1904 (M 79)	2.12 ± 0.64	-0.02 ± 0.64	12.20	207.50 ± 0.50
NGC 2808	0.58 ± 0.45	2.06 ± 0.46	9.60	$93.60 \pm N/A$
NGC 3201	5.28 ± 0.32	-0.98 ± 0.33	5.00	$494.00 \pm N/A$
NGC 4372	-6.49 ± 3.71	3.71 ± 0.32	5.80	$72.30 \pm N/A$
NGC 4590 (M 68)	-3.76 ± 0.66	1.79 ± 0.62	8.90	-95.10 ± 0.60
NGC 4833	-8.11 ± 0.35	-0.96 ± 0.34	6.50	$200.20 \pm N/A$
NGC 5024 (M 53)	0.50 ± 1.00	-0.10 ± 1.00	17.90	-79.10 ± 4.10
ω Centauri (NGC 5139)	-5.08 ± 0.35	-3.57 ± 0.34	4.90	232.50 ± 0.70
NGC 5272 (M 3)	-1.10 ± 0.51	-2.30 ± 0.54	9.50	-147.10 ± 0.40
NGC 5904 (M 5)	5.07 ± 0.68	-10.70 ± 0.56	7.20	51.80 ± 0.50
NGC 5927	-5.72 ± 0.39	-2.61 ± 0.40	7.60	$-107.50 \pm N/A$
NGC 5986	-3.81 ± 0.45	-2.99 ± 0.37	10.40	$88.90 \pm N/A$
NGC 6093 (M 80)	-3.31 ± 0.58	-7.20 ± 0.67	8.30	7.30 ± 4.10
NGC 6121 (M 4)	-12.50 ± 0.36	-19.93 ± 0.49	1.80	70.40 ± 0.40
NGC 6171 (M 107)	-0.70 ± 0.90	-3.10 ± 1.00	5.90	-33.80 ± 0.30
NGC 6205 (M 13)	-0.90 ± 0.71	5.50 ± 1.12	6.80	-246.60 ± 0.90
NGC 6218 (M 12)	1.30 ± 0.58	-7.83 ± 0.62	4.20	43.50 ± 0.60
NGC 6254 (M 10)	-6.00 ± 1.00	-3.30 ± 1.00	4.10	75.50 ± 1.10
NGC 6266	-3.50 ± 0.37	-0.82 ± 0.37	6.90	-70.00 ± 1.30
NGC 6273	-2.86 ± 0.49	-0.45 ± 0.51	8.60	135.00 ± 4.00
NGC 6284	-3.66 ± 0.64	-5.39 ± 0.83	15.30	27.60 ± 1.70
NGC 6287	-3.68 ± 0.88	-3.54 ± 0.69	9.30	-288.80 ± 3.50
NGC 6293	0.26 ± 0.85	-5.14 ± 0.71	8.80	-146.20 ± 1.70
NGC 6304	-2.56 ± 0.29	-1.56 ± 0.26	6.10	-107.30 ± 3.60
NGC 6316	-2.42 ± 0.63	-1.71 ± 0.56	11.00	71.50 ± 8.90
NGC 6333	-0.57 ± 0.57	-3.70 ± 0.50	7.90	229.10 ± 7.00
NGC 6341 (M 92)	-3.30 ± 0.55	-0.33 ± 0.70	7.40	-120.50 ± 1.70

Continues on next page ...

Continued from previous page.

Name	$\mu_{\alpha cos(\delta)}$ (mas yr^{-1})	μ_{δ} (mas yr^{-1})	$R_{\odot}$ kpc	V_{rad} (km s^{-1})
NGC 6342	-2.77 ± 0.71	-5.84 ± 0.65	8.60	116.20 ± 1.60
NGC 6356	-3.14 ± 0.68	-3.65 ± 0.53	15.20	27.00 ± 4.30
NGC 6388	-1.90 ± 0.45	-3.83 ± 0.51	10.00	81.20 ± 1.20
NGC 6397	3.69 ± 0.29	-14.88 ± 0.26	2.30	18.80 ± 0.10
NGC 6441	-2.86 ± 0.45	-3.45 ± 0.76	11.70	16.40 ± 1.20
NGC 6540	0.07 ± 0.40	1.90 ± 0.57	3.70	-17.72 ± 1.40
NGC 6552	3.35 ± 0.60	-1.19 ± 0.34	7.80	-21.10 ± 3.40
NGC 6558	-0.12 ± 0.55	0.47 ± 0.60	7.40	-197.20 ± 1.50
NGC 6626	0.63 ± 0.67	-8.46 ± 0.67	5.50	17.00 ± 1.00
NGC 6652	4.75 ± 0.07	-4.45 ± 0.10	9.60	-111.70 ± 5.80
NGC 6656	7.37 ± 0.50	-3.95 ± 0.42	3.20	-146.30 ± 0.20
NGC 6715	-2.14 ± 0.20	0.03 ± 0.20	28.40	53.30 ± 0.80
NGC 6723	-0.17 ± 0.45	-2.16 ± 0.50	8.80	-94.50 ± 3.60
NGC 6779 (M 56)	0.30 ± 1.00	1.40 ± 0.10	9.40	-135.90 ± 0.90
NGC 6809 (M 55)	-1.42 ± 0.62	-10.25 ± 0.64	5.00	174.90 ± 0.40
NGC 6838 (M 71)	-2.30 ± 0.80	-5.10 ± 0.80	3.60	-22.90 ± 0.20
NGC 7078 (M 15)	-0.95 ± 0.51	-5.63 ± 0.50	9.50	-106.60 ± 0.60
NGC 7089 (M 2)	5.90 ± 0.86	-4.95 ± 0.86	11.20	-3.10 ± 0.90
NGC 7099 (M 30)	1.42 ± 0.69	-7.71 ± 0.65	7.30	-184.30 ± 1.00
NGC 1851	1.28 ± 0.68	2.39 ± 0.65	11.30	320.50 ± 0.60
NGC 2298	4.05 ± 1.00	-1.72 ± 0.98	9.30	149.40 ± 1.30
NGC 288	4.40 ± 0.23	-5.62 ± 0.23	7.60	-46.40 ± 0.40
NGC 362	5.07 ± 0.71	-2.55 ± 0.72	7.80	223.50 ± 0.50
NGC 4147	-1.85 ± 0.82	-1.30 ± 0.82	16.40	183.00 ± 1.00
NGC 5466	-4.65 ± 0.82	0.80 ± 0.82	15.40	107.70 ± 0.30
NGC 5897	-4.93 ± 0.86	-2.33 ± 0.84	12.40	101.70 ± 1.00
NGC 6144	-3.06 ± 0.64	-5.11 ± 0.72	9.00	189.40 ± 1.10
NGC 6362	-3.09 ± 0.46	-3.83 ± 0.46	6.80	-13.30 ± 0.60
NGC 6584	-0.22 ± 0.62	-5.79 ± 0.67	12.90	222.90 ± 15.00

Continues on next page ...

Continued from previous page.

Name	$\mu_{\alpha cos(\delta)}$ (mas yr^{-1})	μ_{δ} (mas yr^{-1})	$R_{\odot}$ kpc	V_{rad} (km s^{-1})
NGC 6712	4.20 ± 0.40	-2.00 ± 0.40	6.50	-107.70 ± 0.60
NGC 6752	-0.69 ± 0.42	-2.85 ± 0.45	3.80	-32.10 ± 1.50
NGC 6934	1.20 ± 1.00	-5.10 ± 1.00	14.90	-412.20 ± 1.60
Palomar 13	2.30 ± 0.26	0.27 ± 0.25	27.20	33.00 ± 20.00
Palomar 6	2.95 ± 0.41	1.24 ± 0.19	7.30	181.00 ± 20.80
Palomar3	0.33 ± 0.23	0.30 ± 0.31	81.60	83.40 ± 8.40
Palomar5	-1.78 ± 0.17	-2.32 ± 0.23	19.90	-55.00 ± 16.00
Terzan 1	0.51 ± 0.31	-0.93 ± 0.29	6.20	114.00 ± 14.00
Terzan 2	-0.94 ± 0.30	0.15 ± 0.42	8.70	109.00 ± 15.00
Terzan 4	3.50 ± 0.69	0.35 ± 0.58	9.10	-5.00 ± 2.90
Terzan 9	0.00 ± 0.38	-3.07 ± 0.49	7.70	59.00 ± 10.00

3 Interstellar Extinction

The existence of absorption of light in the interstellar medium (ISM) was a matter of debate until Trumpler (1930) presented conclusive proof. With the assumption that open clusters of similar degrees of star concentration would have the same dimensions, regardless of their distance from the Sun, Trumpler estimated their distances by comparing their angular diameters to their expected linear diameters. If no interestellar extinction existed, distances found by this method would agree with photometric distances. Yet, he found they did not. The further the object was from the Sun, the greater was the overestimation of its photometric distance. It is now known that not only the ISM is permeated by dust, but that the composition and density of this dust varies considerably throughout the Galaxy, producing different degrees of extinction and reddening depending on the line of sight.

Extinction, which is a dimming of magnitude, is defined as the difference between the observed and intrinsic magnitudes of an object in a band, e.g. $A_B = B_{observed} - B_{intrinsic}$. The color index of an object is the difference between its magnitudes in two different bands, e.g. $B-V$. The difference between the measured colour index of an object and its intrinsic color is a measurement of reddening, also known as color excess, e.g. $E(B-V) = (B-V)_{observed} - (B-V)_{intrinsic} = A_B - A_V$ in the B and V bands. Both extinction and reddening are deeply intertwined as they originate from the same physical phenomenon, namely the existence of interstellar dust. Another convenient definition is the total to selective extinction R_λ, e.g. $R_V = \frac{A_V}{A_B - A_V} = \frac{A_V}{E(B-V)}$, also known as the ratio of extinction to reddening at λ.

With observational data in various wavelengths, Cardelli, Clayton & Mathis (1989) derived an extinction law $A_{(\lambda)}$ depending solely on the R_V parameter. Fitzpatrick & Massa (2007), however, found that this single parameter dependence only held for a few large values of R_V and that, in general, the UV and IR portions of the extinction curves are not correlated and show large variations in different lines of sight. The difference between various extinction curves is notoriously large

in the UV, but changes in the IR region are significantly smaller (Nishiyama et al., 2006, and references therein) and make those bands ideal for determination of GC parameters such as age and distance.

With the uniqueness of the extinction curve in each line of sight, many works rely on extinction maps to derive uncertainties. Multiple authors have presented maps with varied footprints and in different bands, but those are often incompatible with each other and cannot be combined (Marshall et al., 2006, and references therein). Arce & Goodman (1999) offer a warning on the use of one of the most widely adopted large scale maps, Schlegel, Finkbeiner & Davis (1998), which they conclude overestimates reddening by a factor of $1.3 - 1.5$ in regions with $A_V > 0.5$ mag while underestimating it in regions with steep extinction gradients. Using the K_S band, which has around one tenth of the extinction of the visible bands, Marshall et al. (2006) derived extinction values in over 64000 lines of sight in $|l| \leq 100\,\mathrm{deg}$, $|b| \leq 10\,\mathrm{deg}$ in different distances, making a three dimensional extinction map. The most common practice in GC study is, however, to derive extinction values directly from the CMDs, adopting a constant $R_V = 3.1$.

With the development of high resolution IR photometry, not only precision in the determination of GC parameters increased, but also previously undetectable GCs have been discovered. Surveys such as Gaia bring new data into highly obscured regions of the sky, making efforts in deriving even more precise, all-sky maps essential. In the left panel of Fig. 1, the scatter plot of $E(B-V)$ vs l and b shows the trend of GCs being more reddened in the plane of the disk and in the direction of the Galactic centre, as expected. There is also a slightly higher $E(B-V)$ for GCs north of the Galactic centre when compared to the south (right panel of Fig. 1).

3.1 Dust Clouds

Dust clouds are abundant in the plane of the disk. They may have very irregular, filamentary shapes with unclear boundaries. The amount of dust is correlated with the column density of neutral hydrogen (H I), and sometimes they present high enough density to initiate stellar formation. While dust clouds are

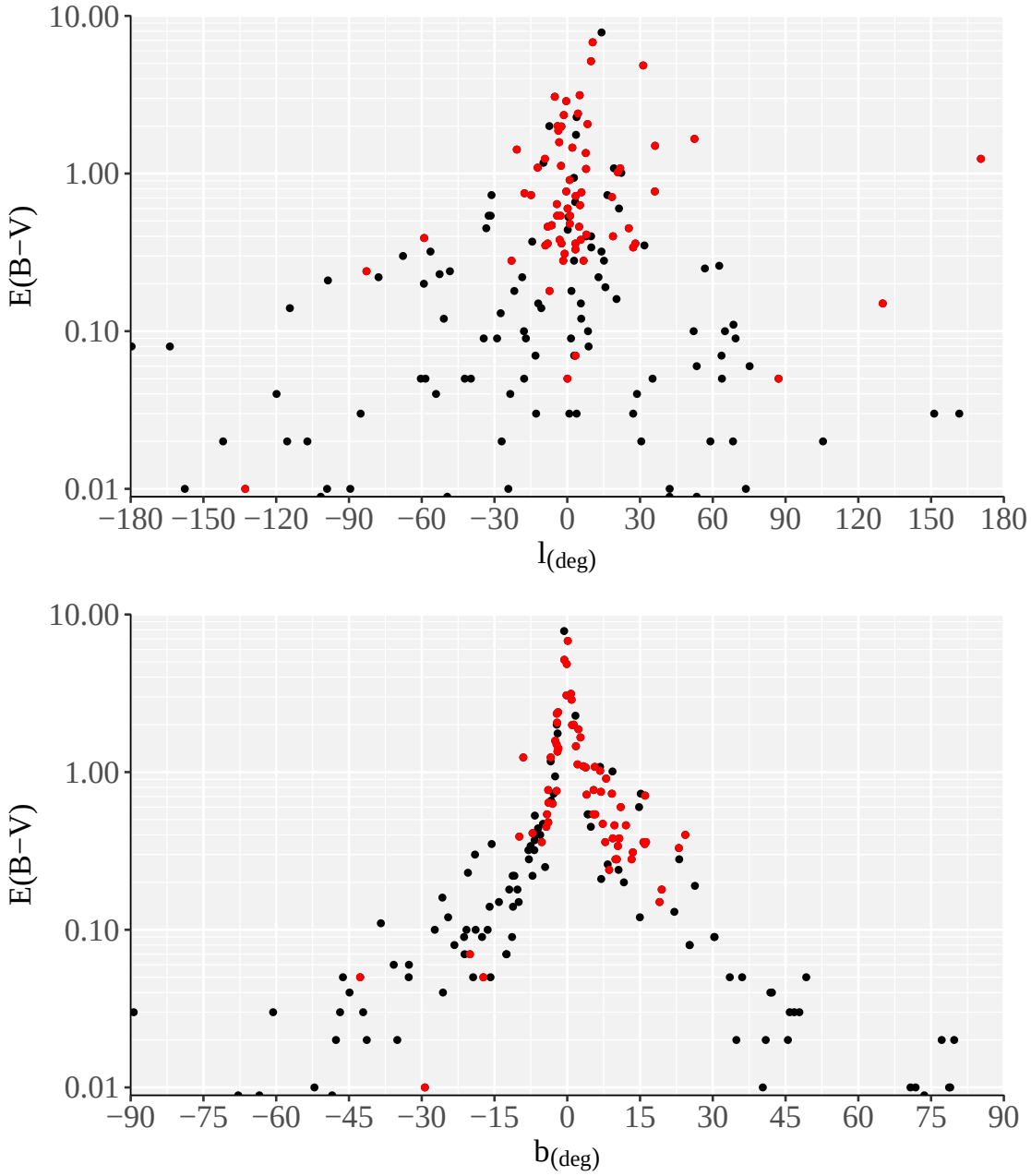

Figure 1 – *Top:* Colour excess $E(B-V)$ versus Galactic longitude l. *Bottom:* Colour excess $E(B-V)$ versus Galactic latitude b. For both panels, GCs behind dust clouds are red. Any objects with $E(B-V) < 0.01$ have no significant color excess, and have been represented over the horizontal axis.

fundamental in the study of Galactic structure, most information regarding them is scattered across many distinct catalogues. Dutra & Bica (2002) (hereafter DB01) collected data for 5004 dust clouds, primarily dark nebulae, cross-identified from 21 catalogues. We have used this unified catalogue to plot an all-sky projection (Figs. 2, 3) and identify which GCs are in the same line of sight as at least one dust cloud (Tab. 4).

Table 4 – GCs that are obscured by dust clouds, including the identification of the latter. For more information, see text.

GC	Dust Cloud
ESO452-SC11	ρ Ophiuchus DN Complex (IREC500)
	Ophiuchus CO Complex
2MASS GC01	LDN303
BH 261	LDN124
Djorg 1	FeSt1-430
	FeSt1-431
FSR 1735	FeSt1-359, HMSTG340.7-2.4C
GLIMPSE-C01	Serpens DN Complex
	Aquila Rift
HP 1 (BH 229)	LDN1741
	FeSt1-431
	LDN1751
	DN1754
IC 1257	Serpens DN Complex
	Aquila Rift
Liller 1	B271
	FeSt1-431
NGC 1904	G228-28.6 (HRK228-29)
NGC 3201	IREC408

Continues on next page ...

Continued from previous page.

GC	Dust Cloud
NGC 4372	FeSt1-199
	Musca DN Complex
	IREC438
NGC 5986	FeSt1-202
	Lupus I
	Lupus DN Complex (Lupus CO Complex)
NGC 6093	ρ Ophiuchus DN Complex (IREC500)
	Ophiuchus CO Complex
NGC 6121	LDN1676 (FeSt1-402)
	ρ Ophiuchus DN Complex (IREC500)
	Ophiuchus CO Complex
NGC 6139	Lupus DN Complex (Lupus CO Complex)
	Lupus VI
	Lupus V
NGC 6144	FeSt1-404
	DN352.97+16.95
	ρ Ophiuchus DN Complex (IREC500)
	Ophiuchus CO Complex
NGC 6171	IREC4
	Upper Scorpius-Ophiuchus DN Complex
NGC 6235	ρ Ophiuchus DN Complex (IREC500)
	Ophiuchus CO Complex
NGC 6256	Lower Scorpius DN Complex (FeSt1-378)
	HMSTG348.0+3.4
NGC 6266	Ophiuchus CO Complex
NGC 6273	Ophiuchus CO Complex
NGC 6284	Ophiuchus CO Complex
NGC 6287	Ophiuchus CO Complex
NGC 6293	Ophiuchus CO Complex

Continues on next page ...

Continued from previous page.

GC	Dust Cloud
NGC 6304	LDN1722
	LDN1741
	Ophiuchus CO Complex
NGC 6316	Ophiuchus CO Complex
NGC 6325	LDN28
	Ophiuchus CO Complex
NGC 6333	Ophiuchus CO Complex
NGC 6342	Ophiuchus CO Complex
NGC 6355	Ophiuchus CO Complex
NGC 6356	Ophiuchus CO Complex
NGC 6366	IREC25
NGC 6401	LDN113
	LDN114 (FeSt1-462)
NGC 6426	IREC44
NGC 6440	LDN246
NGC 6453	FeSt1-430
NGC 6522	LDN3
NGC 6528	LDN3
NGC 6535	Serpens DN Complex
	Aquila Rift
NGC 6539	Aquila Rift
NGC 6544	LDN180 (FeSt1-472)
NGC 6553	LDN176
NGC 6638	LDN245
NGC 6712	Aquila Rift
NGC 6723	Corona Australis DN Complex (R Cra CO Complex)
NGC 6749	Aquila Rift
	LDN624
NGC 6760	Aquila Rift
	B138 (LDN627)

Continues on next page ...

Continued from previous page.

GC	Dust Cloud
Palomar 1	−12 Km/s CO Clouds
	Lindblad Ring
Palomar 2	Taurus DN Complex (Taurus CO Complex)
Palomar 6	LDN34
	LDN82
Palomar 10	CO Cloud B
	CO Cloud C
Palomar 13	MBM55
Palomar 15	IREC24 (MBM151)
Terzan 1 (HP 2)	FeSt1-431
	LDN1769
Terzan 2 (HP 3)	LDN1741
	FeSt1-431
Terzan 3	Lupus DN Complex (Lupus CO Complex)
	Lupus V
Terzan 4 (HP 4)	LDN1732
	FeSt1-431
Terzan 6 (HP 5)	FeSt1-431
Terzan 7	Corona Australis DN Complex (R Cra CO Complex)
Terzan 10	FeSt1-467
	LDN150 (FeSt1-465)
Terzan 12	FeSt1-483
	FeSt1-485
	CB116
Tonantzintla 2 (Pismis 26)	FeSt1-399
UKS 1	LDN150 (FeSt1-465)

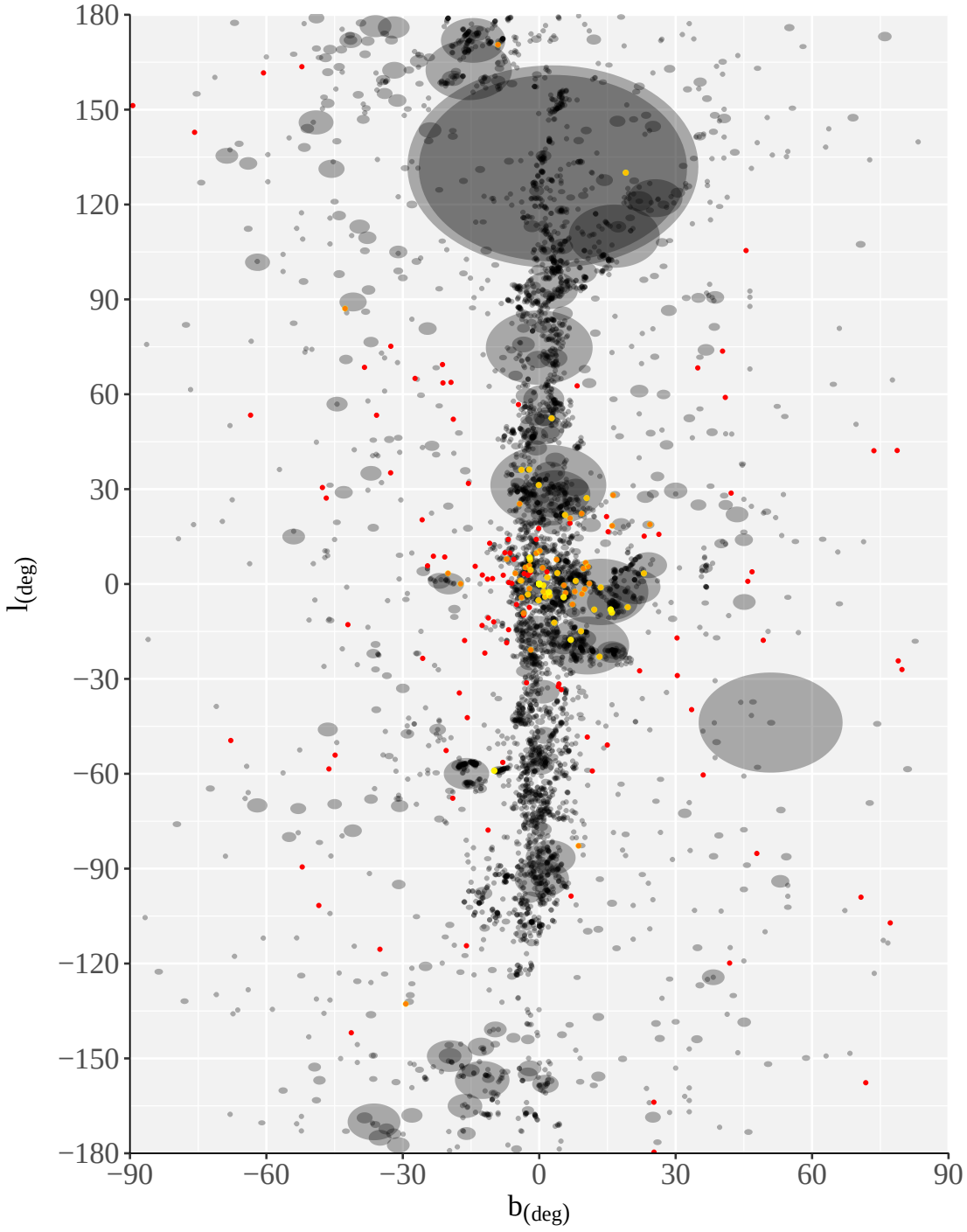

Figure 2 – All sky map of dust clouds (grey ellipses) and GCs (red dots). Clouds with a radius smaller than 0.8° are represented as dots. Obscured GCs have a yellow overlay with intensity proportional to the number of dust clouds in their line of sight.

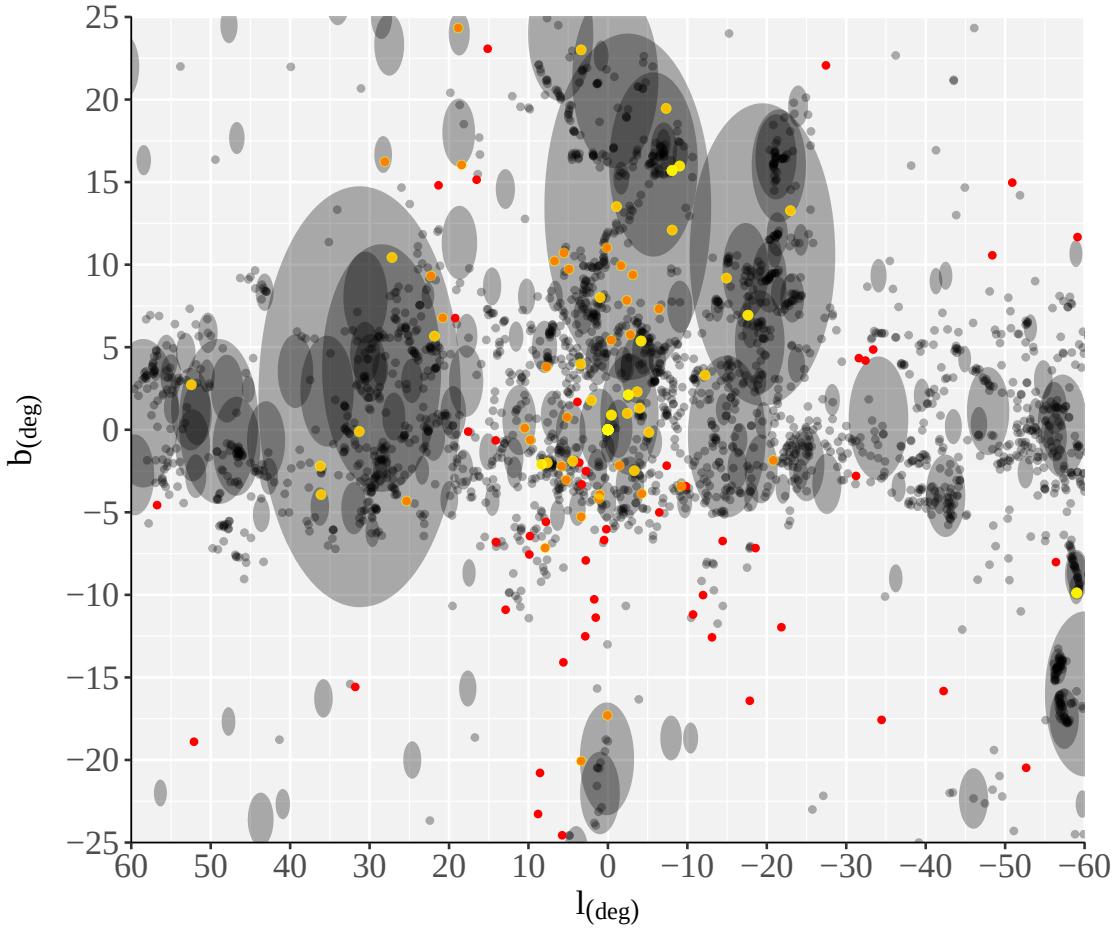

Figure 3 – Same as Fig. 2, for the central part of the Galaxy.

It is difficult to precisely represent the shape of the dust clouds. DB01 defines their boundaries as an ellipse with a minor and major axes. We have taken only the latter measurement, approximating their shapes for transluscent circles so the stacking of multiple dark clouds can be easily identified. Tab. 4 lists all GCs that are in the same line of sight as any given dark cloud.

We verified, by checking 2MASS images that GCs with $E(B-V) > 1.0$ mag are all behind at least one dark cloud despite the few false negatives given by the automated search program. This is due to the circular shape approximation, that only roughly represents the true shape of the highly irregular clouds. The higher values of $E(B-V)$ north of the disk (Fig. 1) correspond to the higher

density of the clouds in that area. In depth studies of the composition of dust clouds can aid in deriving a specific extinction law for the GCs obscured by them. The fact that we found up to 3 dust clouds in some GCs lines of sight indicates that caution should be taken in adopting a single extinction law, as even multiple R_V values might be present in each cloud, although we do no further exploration of this possibility in the present work. As discussed in 3, widely used extinction maps rely on adopting $R_V = 3.1$, but it is possible that this approximation becomes unrealistic for the GCs that are behind one or more dust clouds.

4 Distance Uncertainty Estimates

H10 presents GC distances, but not their uncertainties. In view of that, we tested different approaches to the computation of those uncertainties, and their effect on the spatial density distributions.

4.1 Error Propagation

Our first test was to use uncertainties in reddening values and horizontal branch magnitude levels to propagate them to distances. GCs in highly reddened regions ($E(B\text{-}V) > 2$) received a particular treament in the near-infrared bands. It is essential to realize that the migration of such observations from the optical to the near-infrared bands to construct CMDs have produced very precise distances. This quality jump is taken into account in the subsequent analysis.

For GCs with reddening values in the range $0.0 < E(B\text{-}V) < 2.0$, the distance uncertainties were propagated from the uncertainties in their reddening values and absolute magnitudes in the horizontal branch, following Eq. 4.1. According to H10, the uncertainty in horizontal branch absolute magnitude is $\sigma M_{V(HB)} \approx 0.1$ mag. This holds true even for the worst cases of errors in the apparent magnitudes. The value adopted for the total to selective absorption R_V was 3.1 (Cardelli; Clayton; Mathis, 1989). Ferraro et al. (1999) performed a homogenous systematic analysis of 61 GCs, finding errors in $E(B\text{-}V)$ smaller than 20%. We verified that the trend continues with larger reddening values (e.g. Ortolani; Bica; Barbuy, 1996; Moni Bidin et al., 2011). We finally assumed $\sigma E(B\text{-}V) = 0.20 \cdot E(B\text{-}V)$ as a comfortable upper limit. Thus we derived the uncertainties in the distance from the Sun

$$\sigma_{d_\odot} = 0.461 \cdot d_\odot \cdot \sqrt{(R_V \cdot \sigma_{E(B-V)})^2 + (\sigma_{M_{V(HB)}})^2} \tag{4.1}$$

GCs in the large reddening domain ($E(B\text{-}V) > 2.0$) are not as a rule visible in optical bands. Since they have been studied, as a rule, in the near-IR, Eq. 4.1

was adapted to the K band with *E(J-K)*, where $R_K = 0.618$ (Dutra; Santiago; Bica, 2002) and $\sigma_{M_{K(HB)}} = 0.1$. The latter value was taken from a comparison of CMDs in the near-IR (Valenti; Ferraro; Origlia, 2007, e.g.).

The resulting error bars in a xy plane projection were clearly overestimated (Fig. 5), specially for nearby GCs, making inferences about Galactic structure considerably difficult. Adding an uncertainty term σ_{R_V} would only increase the distance uncertainties. Adopting a smaller factor for $\sigma_{E(B-V)}$, of 10% to 15% at most, would decrease the distance uncertainties significantly, but doing so could introduce unrealistic values. Therefore, we opted to gather distance uncertainties given in various papers to analyse how they scale with distance.

4.2 Uncertainty Values in the Literature

We gathered distance uncertainty values given in the literature for various GCs (Tab. 5). Plotting those uncertainties versus distance values, a linear fit provided a value $\sigma_{d_\odot} = 0.07 \pm 0.01$. Therefore, we have adopted the 10% value for the confidence intervals of the distributions in each direction. xy plane projections of GCs with the error bars are presented in Fig. 5, for both the literature uncertainty values and the adopted 10% uncertainties. It is important to note that these uncertainties were only used for the derivation of the confidence interval for the position distributions. In Sect. 7.4.1 we perform further probing on the uncertainty values and how they relate to detected asymmetries in plane projections.

Table 5 – Distance uncertainty values gathered from literature. References are at the end of the table.

Name	$d_{\odot(kpc)} \pm \sigma_{d_{\odot}(kpc)}$	Reference
FSR 1767	1.50 ± 0.10	[1]
NGC 6397	2.39 ± 0.13	[2]
NGC 6656 (M 22)	2.84 ± 0.16	[2]
GLIMPSE-C01	3.70 ± 0.80	[3]
NGC 6752	4.02 ± 0.10	[2]

Continues on next page ...

Continued from previous page.

Name	$d_{\odot(kpc)} \pm \sigma_{d_{\odot}(kpc)}$	Reference
47 Tucanae (NGC 104)	4.15 ± 0.08	[2]
Terzan 5 (Terzan 11)	5.10 ± 0.50	[4]
ω Centauri (NGC 5139)	5.19±0.08	[5]
NGC 6266 (M 62)	6.42 ± 0.14	[2]
2MASS GC02	7.10 ± 1.40	[6]
VVV CL002	7.30 ± 0.90	[7]
NGC 5904 (M 5)	7.79 ± 0.61	[2]
Liller 1	7.80 ± 1.30	[4]
NGC 5927	7.91 ± 0.88	[2]
Kronberger 49	8.00 ± 1.00	[8]
Terzan 4 (HP 4)	8.00 ± 3.00	[4]
NGC 6723	8.47 ± 0.17	[9]
NGC 6341 (M 92)	8.93 ± 0.31	[2]
NGC 288	9.03 ± 0.56	[2]
NGC 2808	9.45 ± 0.15	[2]
Terzan 10	10.30 ± 0.40	[6]
NGC 1851	10.32 ± 0.24	[2]
NGC 7078 (M 15)	10.36 ± 0.16	[2]
NGC 6388	10.90 ± 0.45	[2]
UKS 1	11.10 ± 1.80	[4]
Pfleiderer 2	16.00 ± 2.00	[10]
Kim 1	19.80 ± 0.90	[11]
NGC 6715 (M 54)	22.57 ± 0.44	[2]
Whiting 1	29.40 ± 2.00	[12]
Balbinot 1	31.90 ± 1.60	[13]
Koposov 2	33.30 ± 1.50	[14]
Koposov 1	34.90 ± 1.60	[14]
Muñoz 1	45.00 ± 5.00	[15]
Laevens 3	67.00 ± 3.00	[16]
Palomar 14 (AvdB)	71.00 ± 2.00	[17]

Continues on next page ...

Continued from previous page.

Name	$d_{\odot(kpc)} \pm \sigma_{d_{\odot}(kpc)}$	Reference
NGC 2419	87.50 ± 3.30	[18]
Kim 2	104.70 ± 4.10	[19]
Laevens 1 (Crater)	145.00 ± 17.00	[20]

[1] Bonatto et al. (2009); [2] Watkins et al. (2015); [3] Ivanov, Kurtev & Borissova (2005); [4] Ortolani et al. (2007); [5] Watkins et al. (2015); [6] Alonso-García et al. (2015), [7] Moni Bidin et al. (2011); [8] Ortolani et al. (2012); [9] Lee et al. (2014); [10] Ortolani et al. (2009); [11] Kim & Jerjen (2015); [12] Carraro, Zinn & Moni Bidin (2007); [13] Balbinot et al. (2013); [14] Paust, Wilson & van Belle (2014); [15] Muñoz et al. (2012); [16] Laevens et al. (2015); [17] Sollima et al. (2011); [18] Di Criscienzo et al. (2011); [19] Kim et al. (2015); [20] Laevens et al. (2014).

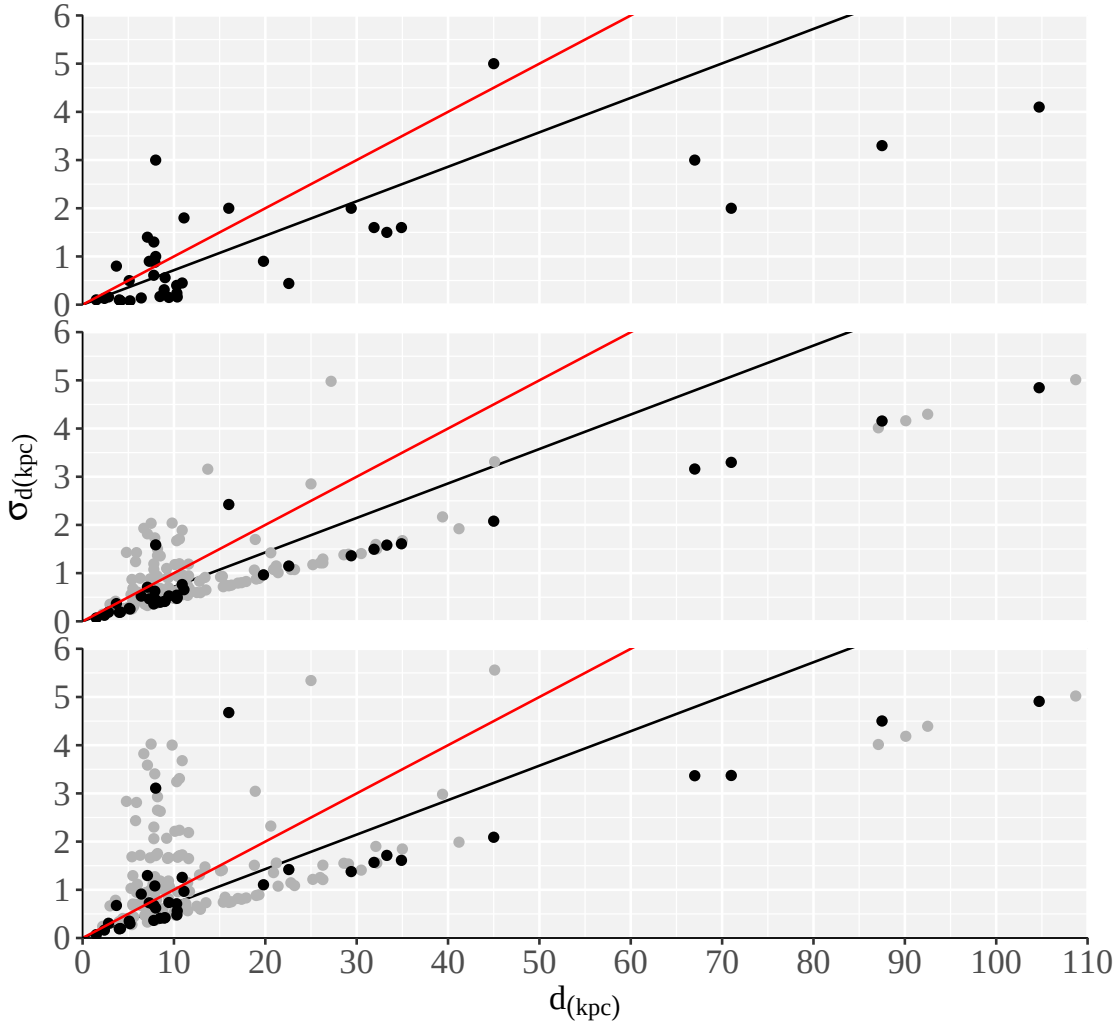

Figure 4 – Effects of different distance uncertainty assumptions. *Top:* Uncertainties gathered from the literature. The black line marks the mean value of 7%, while the red line marks the adopted value of 10%. These two lines remain the same in the three panels. *Middle:* Uncertainties derived from the error propagation formula (Eq. 4.1), with $\sigma E(B-V) = 0.10E(B-V)$. Black dots represent the same sample as the top panel. *Bottom:* Same as the middle panel, but for $\sigma E(B-V) = 0.20E(B-V)$.

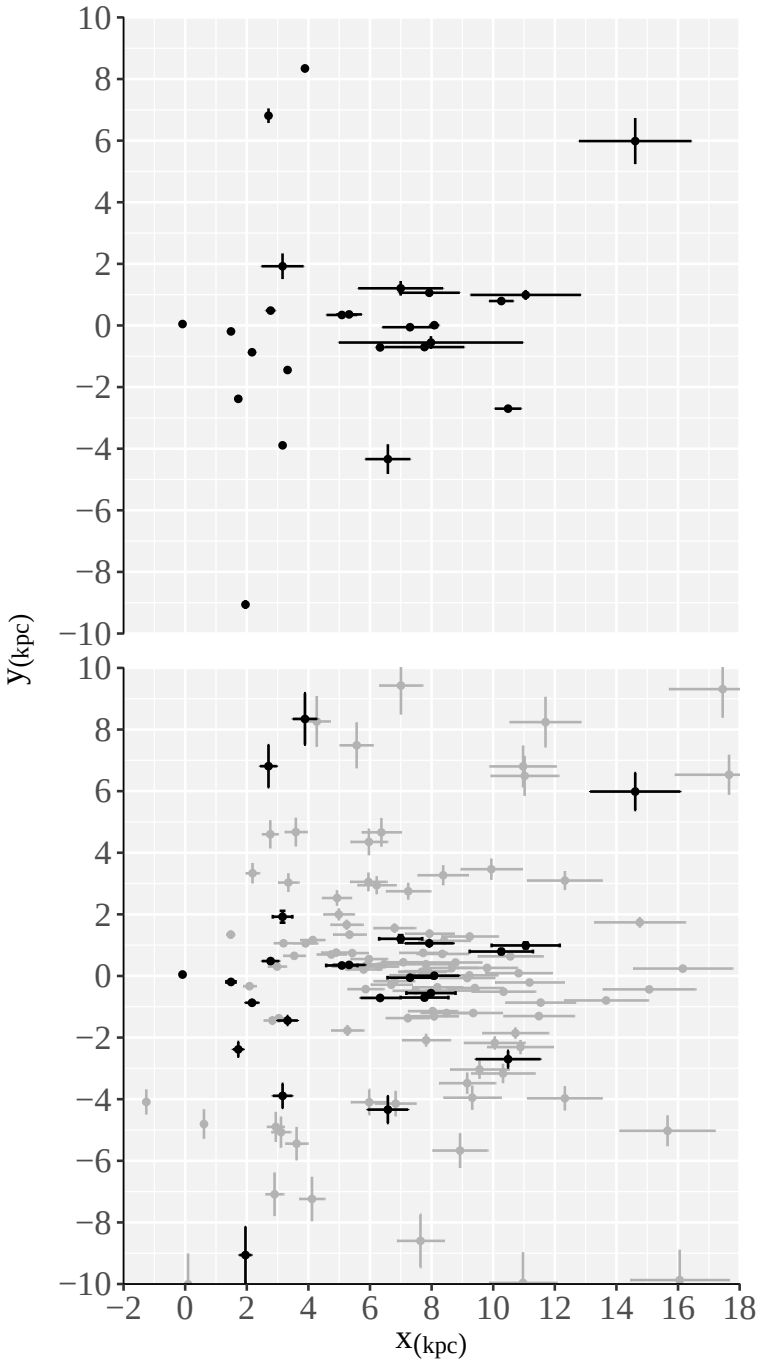

Figure 5 – Comparison between the uncertainties gathered from the literature (top) and calculated from the adopted value of $\sigma_{d_\odot} = 0.10 d_\odot$ (bottom) in a x, y plane projection. In the bottom panel, GCs in the same sample as the top panel are black.

5 Subsamples

In this section we derive subsamples for the GCs according to metallicity, distance from the Galactic plane, or shared characteristics that deviate from typical GC properties.

5.1 Retrograde, Young, and Related to Accretions

In this subsample we removed from the full sample GCs that have special characteristics such as young age or are unlikely to have been formed in the Galaxy. With the assumption that native and old GCs form a mostly symmetrical distribution, these objects could be the cause of asymmetries, which is the hypothesis we seek to test. As a first step, we used the classification by B06: Y - Younger than 10 Gyr, R - Retrograde orbit, S - Sagittarius, C - Canis Major, DN - Dwarf Nucleus, ST - Sagittarius Tidal tail, CT - Canis Major Tidal tail. The groups S, C, DN, ST, CT were combined into Related to Dwarf Galaxies (RDG). The RDG group has 14 GCs, while Y has 17 GCs and R has 15.

As a second step, we used the relative ages derived by Marín-Franch et al. (2009) to include more GCs in the Y group and create the O (relatively old, with 41 GCs) group. This new classification differs from B06 on two objects: NGC 6352 and NGC 6366, which B06 considers young while Marín-Franch et al. consider old. We have adopted classification from the latter work, totalling 38 GCs. While the aforementioned work is interested in studying relative ages, it does present some estimates for different models. With the models from Dotter et al. (2007), the old group has a mean age of 12.8 Gyr and no age-metallicity relation, with a short age spread that suggests a fast halo formation process lasting ~ 0.8 Gyr. The young group shows a clear age-metallicity relationship, with a larger age spread of ~ 6 Gyr.

There is a total of 81 GCs belonging to one or more groups. We verified that the removal of the RDG and Y groups from the full sample does not create a

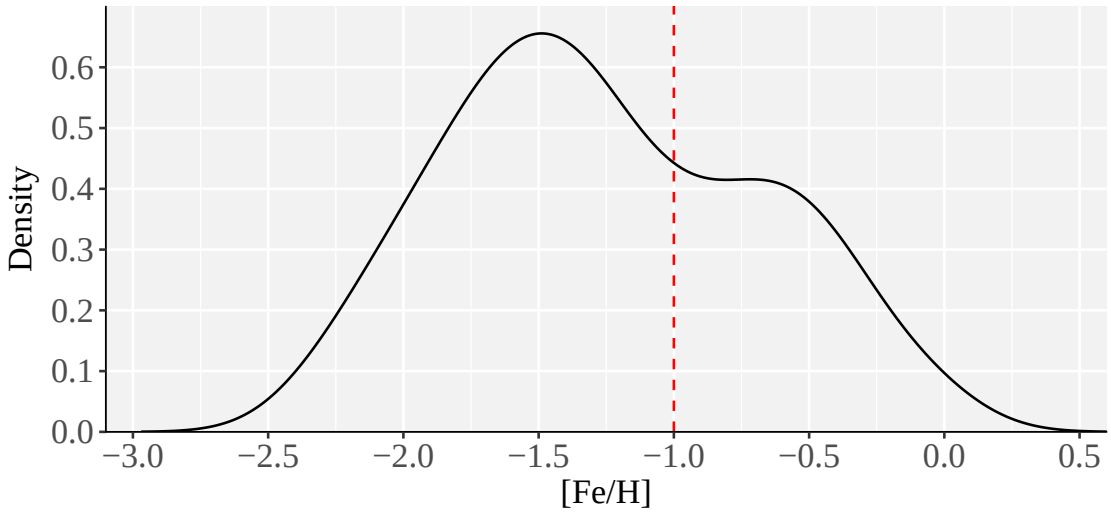

Figure 6 – Observed metallicity distribution of the full sample. The red line is the limit between metal poor and metal rich GCs.

significant change with respect to the full sample spatial distribution characteristics.

5.2 High and Low Metallicities

The adopted threshold between high and low metallicity was $[Fe/H] = -1.0$ to preserve a significant sample size in both metallicity groups, with the 4 GCs with $[Fe/H] = -1.0$ considered high metallicity. This value is close to a minimum in the metallicity distribution (Fig. 6). The sample splitting into high and low metallicity is relevant given the bimodality of the distribution function.

5.3 Small Heights from the Galactic Plane

The GCs with medium and large heights ($|z| > 2.5$ kpc) were removed from the full sample, allowing the examination of GCs about the Galactic plane. This is of particular relevance in this work, as we are interested in exploring how the bulge, bar, and disk could have affected the GC distribution. It is important to note that GCs could be temporarily in this region due to elliptical orbits. The presence of GCs in lower heights could imply that the destruction rate in this region is not

enough to completely destroy some GCs, which would need to be more massive in the past, and that the disk, even if predated by GCs, significantly altered their orbits.

6 Distribution Functions

We have computed the spatial distribution functions for the GCs with two different codes, one in FORTRAN that generates a discrete output, and one in R that generates a continuous output. Both outputs were then analysed with the aid of a fitted Sérsic profile function, which allowed us to extract information about 1) the centroid of the distribution in each direction, 2) the general shape of the distribution (the n parameter of the Sérsic function), and 3) asymmetries that deviated from the expected smooth distribution of a monolithic collapse. The two codes have compatible results (Fig. 8), therefore only images generated from the continuous distribution will be used with the exception of the aforementioned example.

6.1 Discrete Distribution

These spatial distributions were generated by a FORTRAN code, developed by C. Bonatto. Differently from a histogram, the output is the distribution function or density of probability that each GC distance will be found in a given value interval, each one corresponding to a bin. The total number of GCs is retrieved by integrating the final distribution. The bin width is optimized in such a way that each point in the distribution has a minimum signal-to-noise ratio defined by the user. Therefore, the presence of peaks and valleys in the distribution is statistically significant. Due to the limited number of GCs, the minimum signal-to-noise ratio parameter had to be set relatively small in order to preserve enough bins in the distribution, as a compromise.

Since asymmetries were of particular importance in this work, a precise estimation of uncertainties was necessary. The discrete distribution code generated error bars from Poissonic errors, which are solely dependent on the number of objects in each bin. This means that the full sample size is not preserved in the distribution as a whole - e.g. the upper error of a bin can introduce a number

of objects in that bin, without removing that number from the remaining bins. This is a limitation that is inherent to this form of discrete analyses. While the asymmetries could be identified with this approach, the overestimated error bars made their existence uncertain.

6.2 Continuous Distribution

The continuous spatial distributions were generated by an R code, developed by J. Crestani. They are based on kernel density estimation, using Gaussian kernels with bandwidth $BW = 1.0$ unless otherwise noted. The choice of a bandwidth value was visual and qualitatively took into consideration the maximum smoothing that could be achieved without compromising relevant features (Fig. 7). The confidence intervals were estimated via bootstrap sampling, with 1000 samples of 170 GCs. The GC bootstrap samples were created by treating each distance as a Gaussian distribution with μ equal to the distance $d_\odot$ itself, and σ equal to the uncertainty $\sigma_{d_\odot}$. Each generated sample would then randomly pick a distance value for each GC from its corresponding Gaussian distribution. Thus, spatial distributions were created for 1000 possibilities of placement for 170 GCs that obeyed the position and position uncertainty of the real sample. They are used for the computation of a confidence interval.

With the distributions for all the bootstrap samples plotted alongside each other, each "slice" of the horizontal axis produced a distribution of its own, that had a confidence interval computed by its cummulative distribution function. With this, a confidence interval for the spatial distribution was determined. Since both discrete and continuous distributions had agreeing results (Fig. 8), the latter has been adopted for the rest of this work.

6.3 Centroids and Shapes of the Distributions

Initially, as explained in Sect. 1, we sought the geometric centre in each coordinate (x, y, z) in the full sample, using a referential centred in the Sun, with x increasing in the direction of the Galactic centre, z in the direction of the Galactic

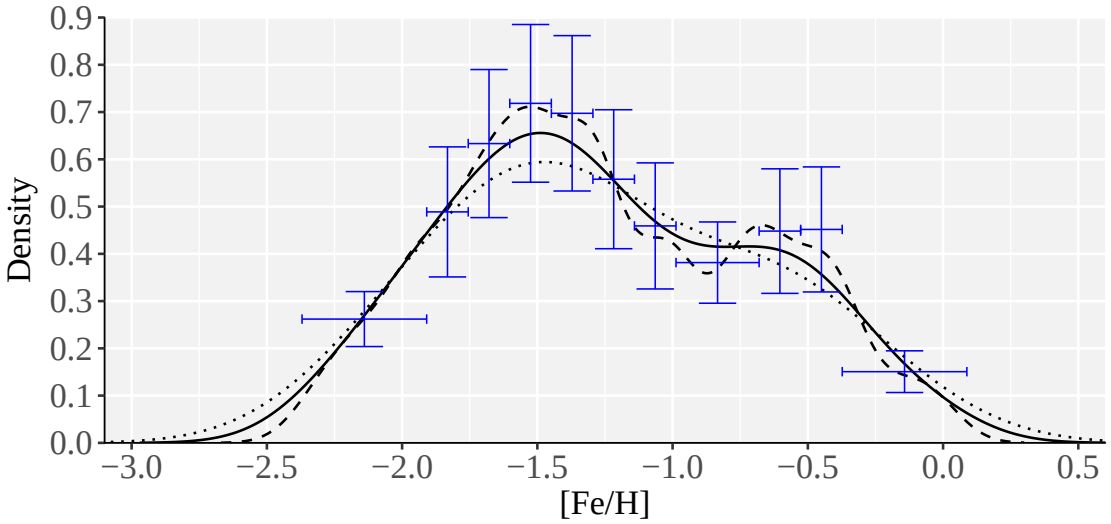

Figure 7 – Comparison between the discrete (blue) and continuous distributions (black). For the continuous distribution, three different bandwidth values were used to illustrate the effect they have on the smoothness and definition of the distribution. The values were 0.1 (dashed line), 0.2 (full line) and 0.3 (dotted line).

North Pole, and y tangent to the disk producing a right-handed coordinate system. This was done via the fitting of a Sérsic Profile function (Eq. 9) to the central region in each direction ($|x| \approx 20$ kpc). The equation below illustrates the distribution function for the x direction

$$\Phi_{(x)} = a \cdot e^{-\left(\frac{|x-b|}{c}\right)^{\frac{1}{n}}} \tag{6.1}$$

where n holds information about the structure and b its centroid. a and c are responsible for the amplitude and width of the distribution, respectively. Note that the Sérsic profile has been used to study the structure of galaxies in the plane of the sky, which is not Cartesian, and is a function of luminosity and not number of objects. Therefore, care must be taken in the interpretation of the n parameter (e.g. certain values of n being representative of a disk or a bulge). In this study, the Sérsic profile function was used as a mathematical tool to derive the centre of each spatial distribution, leaving the n parameter free in order to optimize the fits.

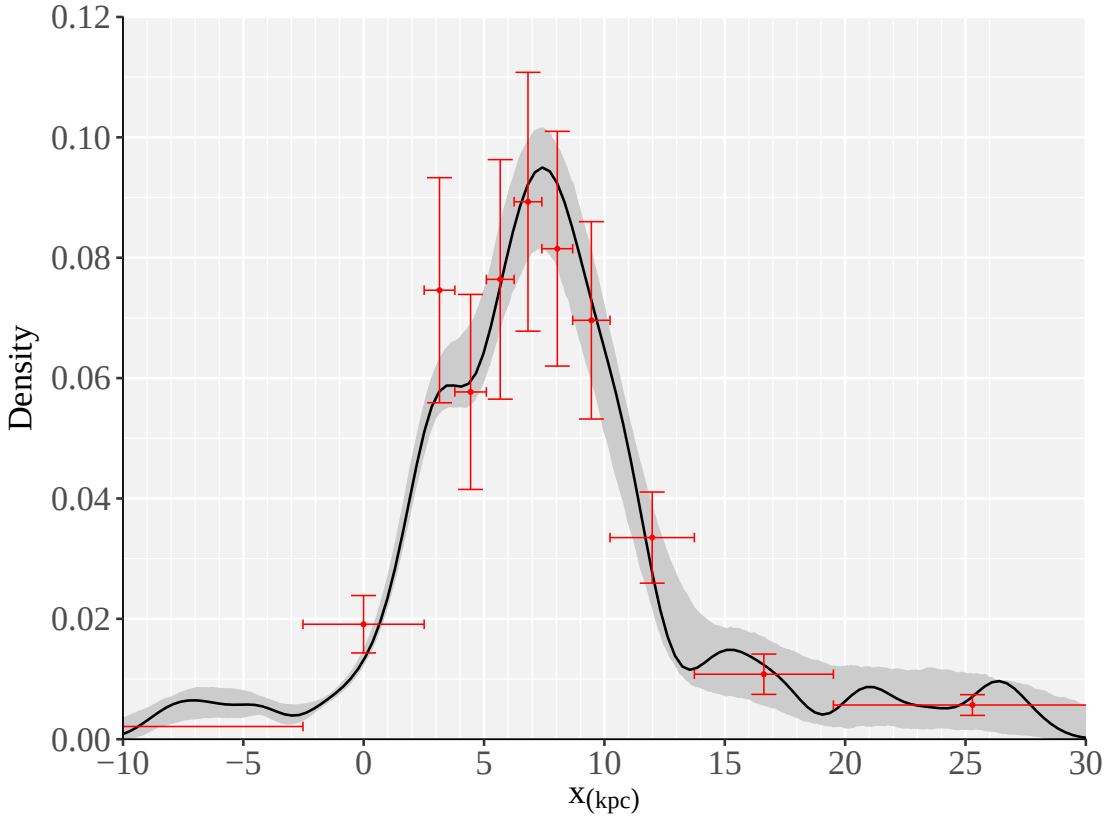

Figure 8 – Comparison between the discrete (red) and continuous distributions (black). The confidence interval for the continuous distribution, displayed in grey, is where the errors derived in Sect. 4 are considered.

7 Results

We explored the spatial distribution in each axis for the full sample with Sérsic profile functions (Eq. 9). We aimed to find their centroids and n parameters. After comparing the distance value found for x_0 (b value for the x direction) with R_0, we focused on the study of the distribution asymmetries by analysing the subsamples (Sect. 5) and how the distributions evolve with time in a Galactic potential.

7.1 Full Sample

We show in Fig. 9 the GC density distributions for the x, y, and z directions. The latter two have peaked spheroidal profiles, drastically different from the wider and flatter one in the x direction. At $x \approx 3$ kpc we detect an interesting GC overdensity that we define as the Secondary Density Peak (SDP). Tab. 6 shows all GCs in the region. A few of them are far in the halo, but most of them stick to the Galactic plane with $|z| < 2.5$ kpc. Those might be interacting with the bar and spiral arms (Fig. 13), a possibility we investigate further in Sect. 7.4.

The spatial distribution of GCs offers a value to be considered for R_0. For the full sample, we found a distance of 7.41 ± 0.01 kpc (Tab. 7) to the centroid of the distribution, in (x, y, z). This value is somewhat smaller than recent estimates for R_0 using other methods, but in agreement with values derived using the GC system (Sect. 1). For the isolated y and z directions, the centroid was very close to zero, as expected. It is important to note that the surprisingly small uncertainty of ± 0.01 kpc is a consequence of the method of kernel density estimation, which produces smooth distributions that might underestimate error bars in function fittings applied to them.

Table 6 – GCs in the Secondary Density Peak region, by increasing z.

Name	$x_{(kpc)}$	$y_{(kpc)}$	$z_{(kpc)}$	$[Fe/H]$	Groups
NGC 362	3.11	-5.07	-6.21	-1.26	Y, R
NGC 7078 (M 15)	3.90	8.38	-4.77	-2.37	O
E 3	2.90	-7.09	-2.64	-0.83	O
NGC 2808	1.99	-9.20	-1.87	-1.14	C, Y
NGC 6752	3.31	-1.44	-1.73	-1.54	Y
NGC 4372	2.94	-4.90	-1.00	-2.17	
NGC 4833	3.62	-5.44	-0.92	-1.85	O
NGC 6397	2.09	-0.84	-0.48	-2.02	O
NGC 6656 (M 22)	3.13	0.54	-0.42	-1.70	O
NGC 6838 (M 71)	2.19	3.33	-0.32	-0.78	O
NGC 6544	2.98	0.30	-0.12	-1.40	
GLIMPSE-C01	3.16	1.92	-0.01	-1.61	
2MASS GC01	3.54	0.65	0.01		
Palomar 10	3.59	4.67	0.28	-0.10	
NGC 6121 (M 4)	2.09	-0.33	0.61	-1.16	O
NGC 6366	3.19	1.06	0.97	-0.59	O
ω Centauri (NGC 5139)	3.17	-3.90	1.34	-1.53	DN, R, Y
NGC 6254 (M 10)	3.91	1.06	1.72	-1.56	Y
NGC 6205 (M 13)	2.76	4.60	4.65	-1.53	R, Y
NGC 6341 (M 92)	2.51	6.33	4.74	-2.31	O
NGC 5466	3.35	3.03	15.35	-1.98	O
NGC 5053	3.04	-1.37	17.08	-2.27	O
NGC 5024 (M 53)	2.83	-1.45	17.62	-2.10	O

Table 7 – Fitting parameters a, b, c, and n in the x, y, and z directions for the full sample.

Parameter	x	y	z
a	0.100 ± 0.000	0.168 ± 0.005	0.169 ± 0.006
b	7.401 ± 0.005	0.105 ± 0.022	0.006 ± 0.035
c	4.773 ± 0.012	2.296 ± 0.114	2.361 ± 0.120
n	0.795 ± 0.003	1.289 ± 0.048	0.972 ± 0.056

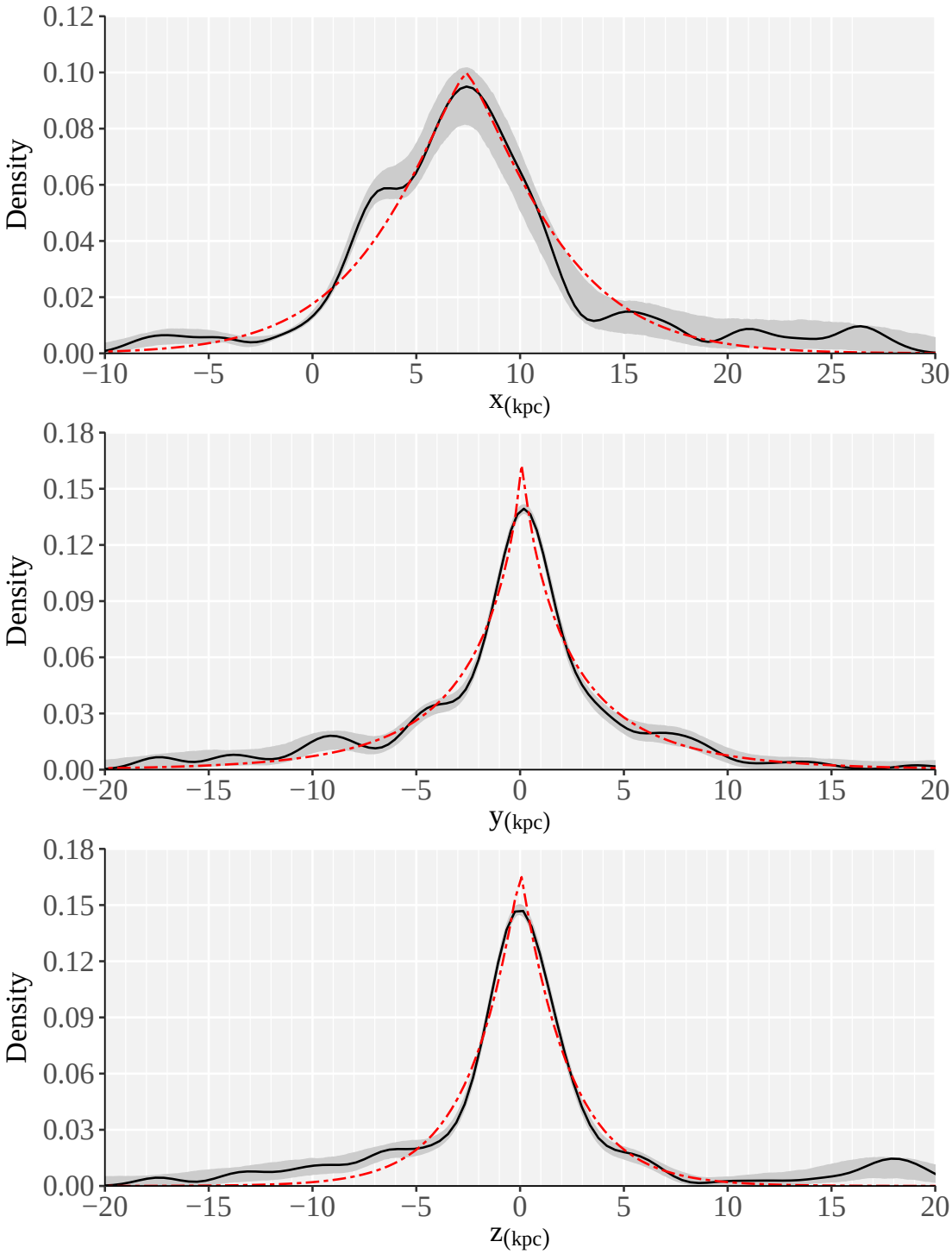

Figure 9 – Density distribution in the three directions (black) with a 0.95 confidence interval for distance uncertainties of 10% (grey) and the Eq. fitting (red).

7.2 High and Low Metallicities

The asymmetry around $x = 3$ kpc essentially belongs to the low metallicity sample (Fig. 10). This is surprising since we expected its distribution to be closer to the fitted function, with the symmetry generated from a monolithic collapse scenario.

7.3 Small Heights from the Galactic Plane

In order to verify if proximity to the disk is significant in the x direction asymmetry (i.e. its flatter and wider shape, and the SDP), we removed medium and large height ($|z| > 2.5$ kpc) GCs from the sample (Fig. 11). There are 23 GCs in this region, and 15 of them stick to the plane (Tab. 6). Most of the characteristics of the distributions in the three directions are created by low height GCs.

7.4 The x Direction Structure

7.4.1 General Shape

There is a clear difference in the shape of the x distribution when compared to the y and z distributions (Fig. 9). Such difference is to be expected if the x direction distribution is more elongated. This could happen if the x direction corresponds to the semi-major axis of an ellipse while y (or z) corresponds to semi-minor axis in a x, y (or x, z) projection. Another possibility is that distances in x are overestimated and/or distances in y and z are underestimated.

To test this first hypothesis, we have made a k axis that coincides with the x axis, centered in the centre of the x distribution ($k = x + 7.4$ kpc), and then rotates in the plane of the disk, generating a new distribution function in this new k direction for each angular step θ, with $\theta \in [0, \pi]$. Thus, $\theta = 0$ defines the x axis, and $\theta = 0.5\pi$ defines the y axis. The resulting distributions can be seen in Fig. 12, where for each θ, the distribution was shifted +1.0 kpc so that all steps could be seen clearly. We have found that the minimum and maximum density values occur for $\theta = 0.94\pi$ ($= -0.6\pi$) and $\theta = 0.46\pi$, respectively. From a purely geometrical

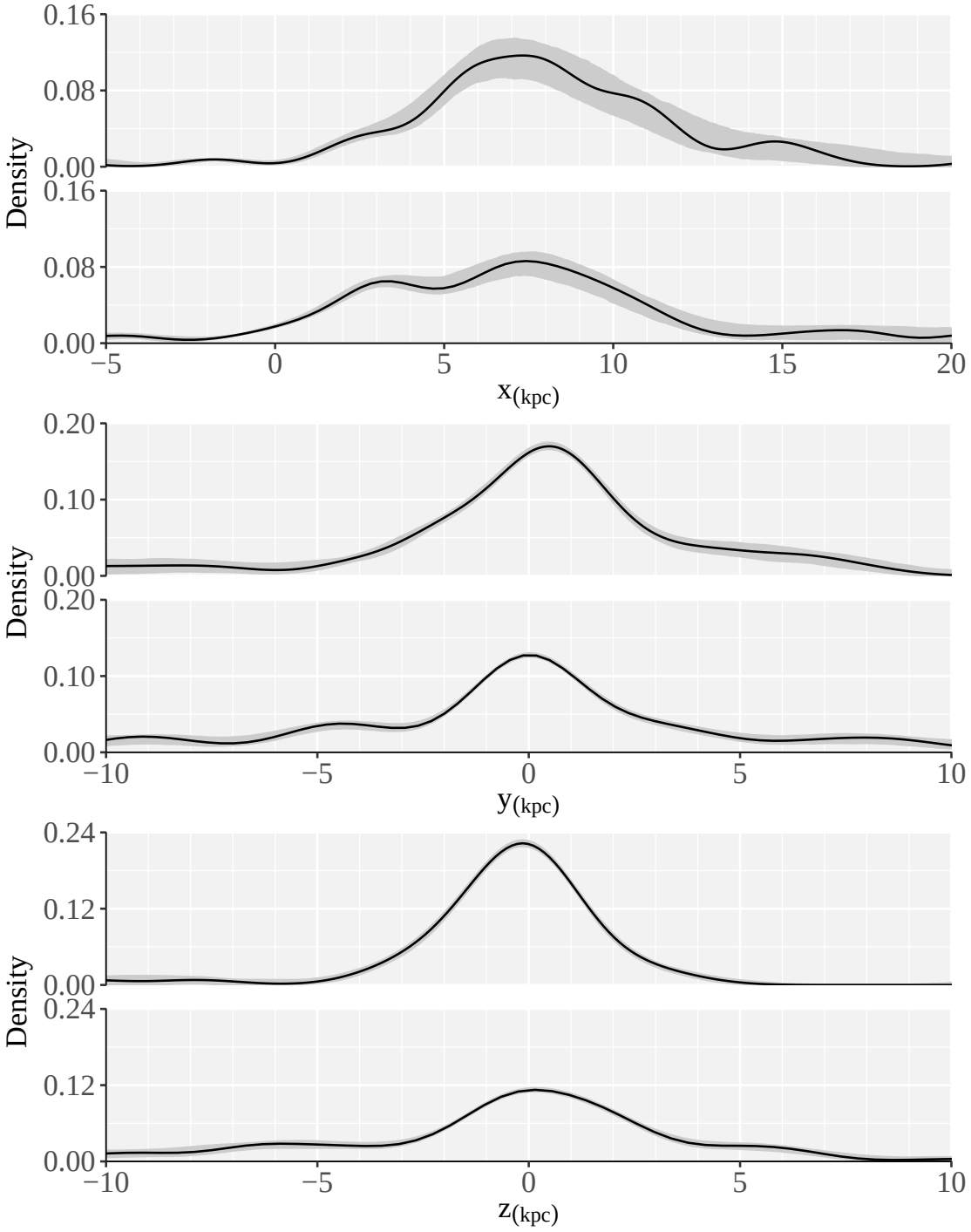

Figure 10 – Spatial distribution of the high metallicity (top of each panel) and low metallicity (bottom of each panel) samples in the x (top panel), y (middle panel), and z (bottom panel) directions.

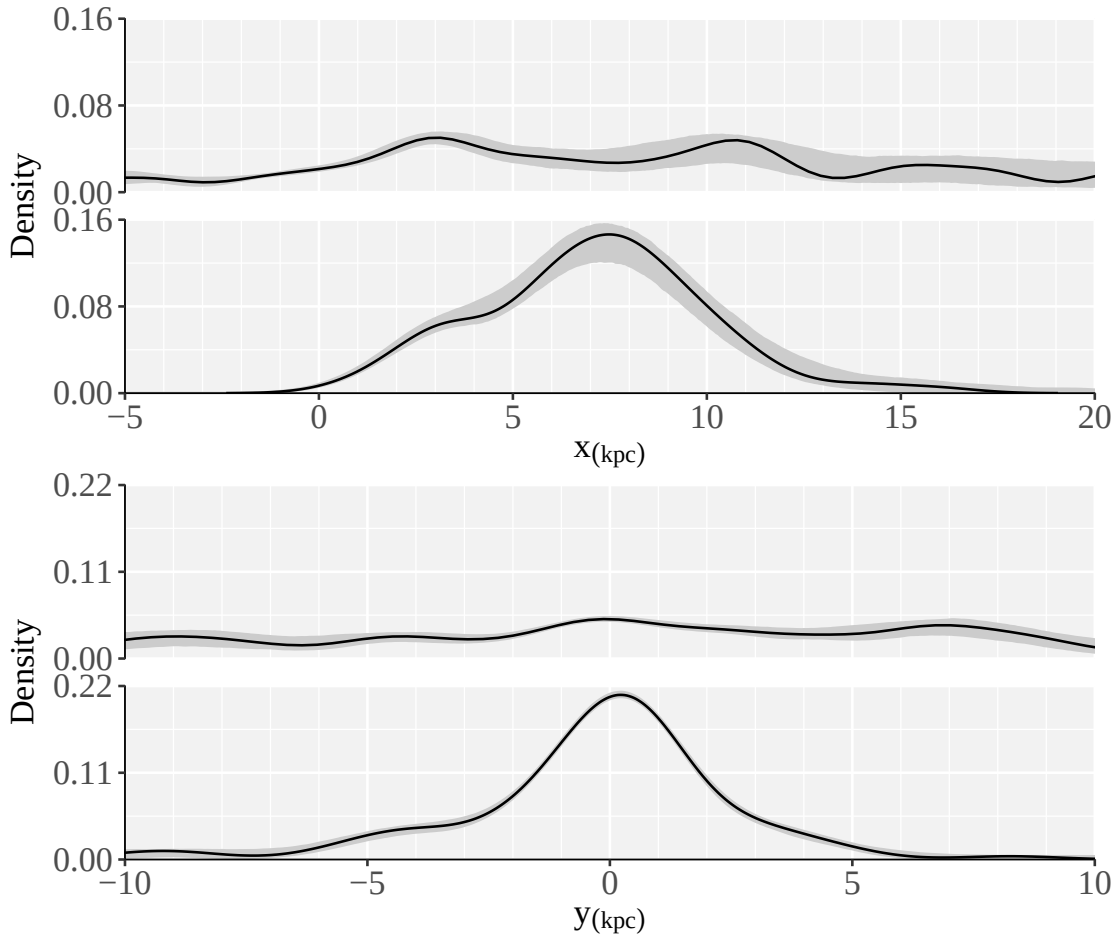

Figure 11 – Spatial distribution in the x (top frame) and y (bottom frame) directions for the $|z| > 2.5$ kpc (top of each frame) and the $|z| \leq 2.5$ kpc (bottom of each frame) samples.

view, these θ values define the minor and major axes of an elliptical distribution. We repeated the same procedure for the x, z and y, z planes (Tab. 8).

To test the second hypothesis (distance overestimation in the x direction), we have remade the distributions using $\alpha d_\odot$ for the computation of the x, y, and z coordinates, where α is a parameter we varied in order to simulate an over- or underestimation of the distance $d_\odot$. Note that the x coordinate cannot change alone, because it is merely a projection of the $d_\odot$ distance that depends on the l and b coordinates, which are very well known. The distributions would only begin

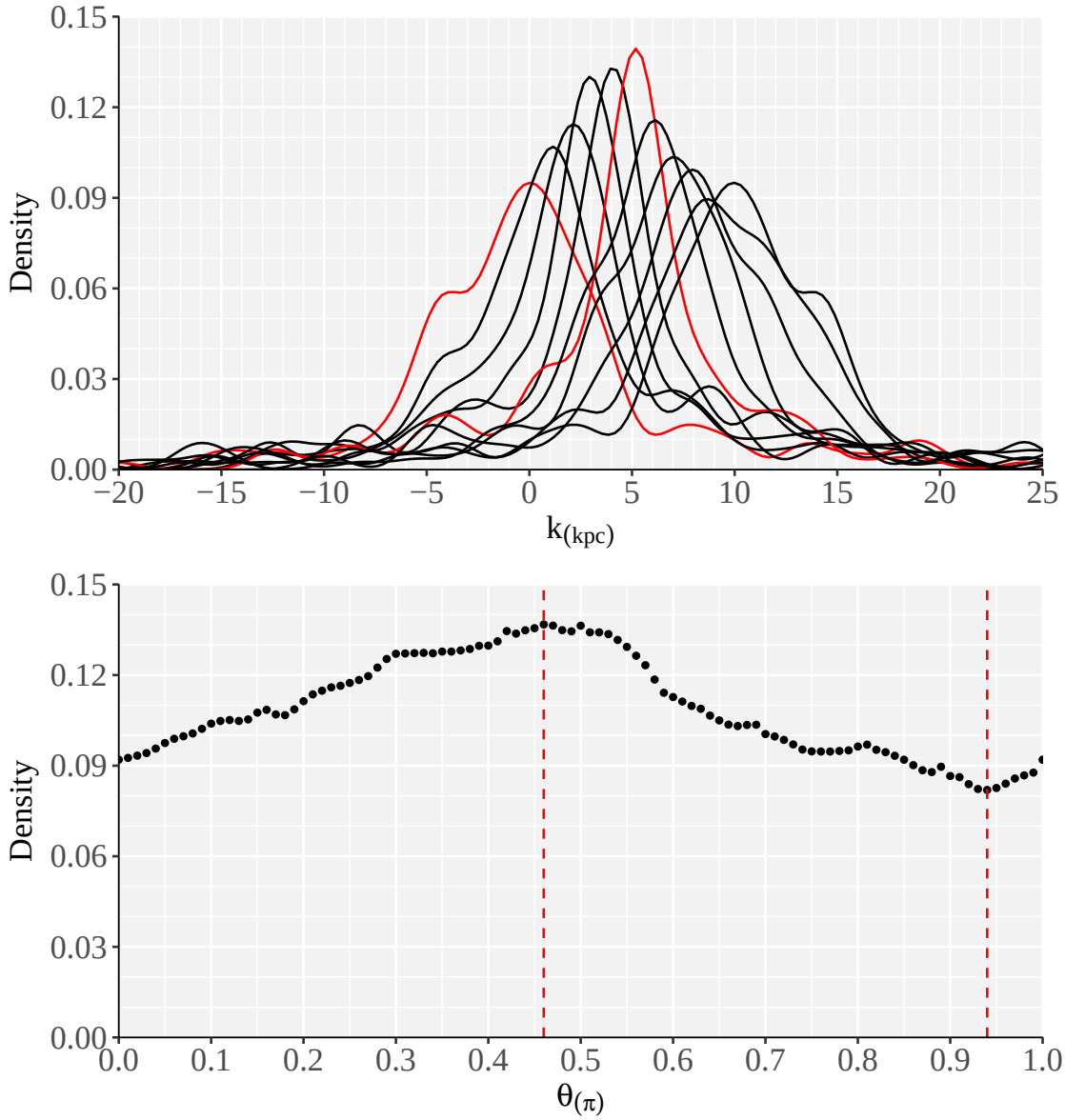

Figure 12 – *Top:* Density distribution in the k direction, with each new k shifted 1 kpc to the right for clarity. In red, the x and y directions for reference. *Bottom:* The peaks of the k direction distribution for each θ. The red dashed lines indicate the maximum and minimum values.

to have similar shapes with $\alpha \leq 0.4$, a value that does not coincide with the current precision of observations.

7.4.2 Plane Projection

To further study the SDP asymmetry and the general shape of the x direction, we computed the (x, y) plane projection of the full GC sample. While the distribution as a whole does not visually appear to be elongated in the x direction, there is a central structure with a strong bar-like shape that is mostly populated by low height ($|z| \leq 2.5$ kpc) GCs (Fig. 13). The GCs present in the SDP are also visually very distinct and are located mostly between two spiral arms.

While the bar-like structure is visually evident, we adopted a statistical approach to analyse its significance. We used the Pearson product-moment correlation coefficient (PPMCC) to compute the correlation between the x and y directions for the low height GCs inside a radius r. Selecting r in a range, we were able to find the radii where the correlation is statistically significant (Fig. 14): $r \in [3.4, 4.3], [4.6, 5.0], [6.0, 6.1]$, with angular orientation varying between $-20°$ and $-28°$. All calculations were done for a confidence interval of 0.95.

This method yielded, for the low height sample, central coordinates $x_0 \in [7.07, 7.36]$ kpc and $y_0 \in [-0.07, 0.09]$ kpc for the statistically significant correlation values. The minimum p-value was 0.003, corresponding to $r = 3.9$ kpc, an angle of $-25.5°$, and axes of length 2.87 and 2.72 kpc for a 0.95 confidence interval. A total of 61 GCs were included in this radius.

We tested the possibility that over- or underestimation of distances could destroy the bar-like structure. Systematic errors, i.e. the same α value for all GCs, do not influence the structure. As the y coordinate is relatively small, a systematic

Table 8 – The θ angle for k, in each plane, for the tallest (corresponding to a minor axis) and shortest (corresponding to a major axis) distributions in the k direction.

	(x, y)	(x, z)	(y, z)
θ_{min}	0.94π	0.02π	0.89π
θ_{max}	0.46π	0.55π	0.61π

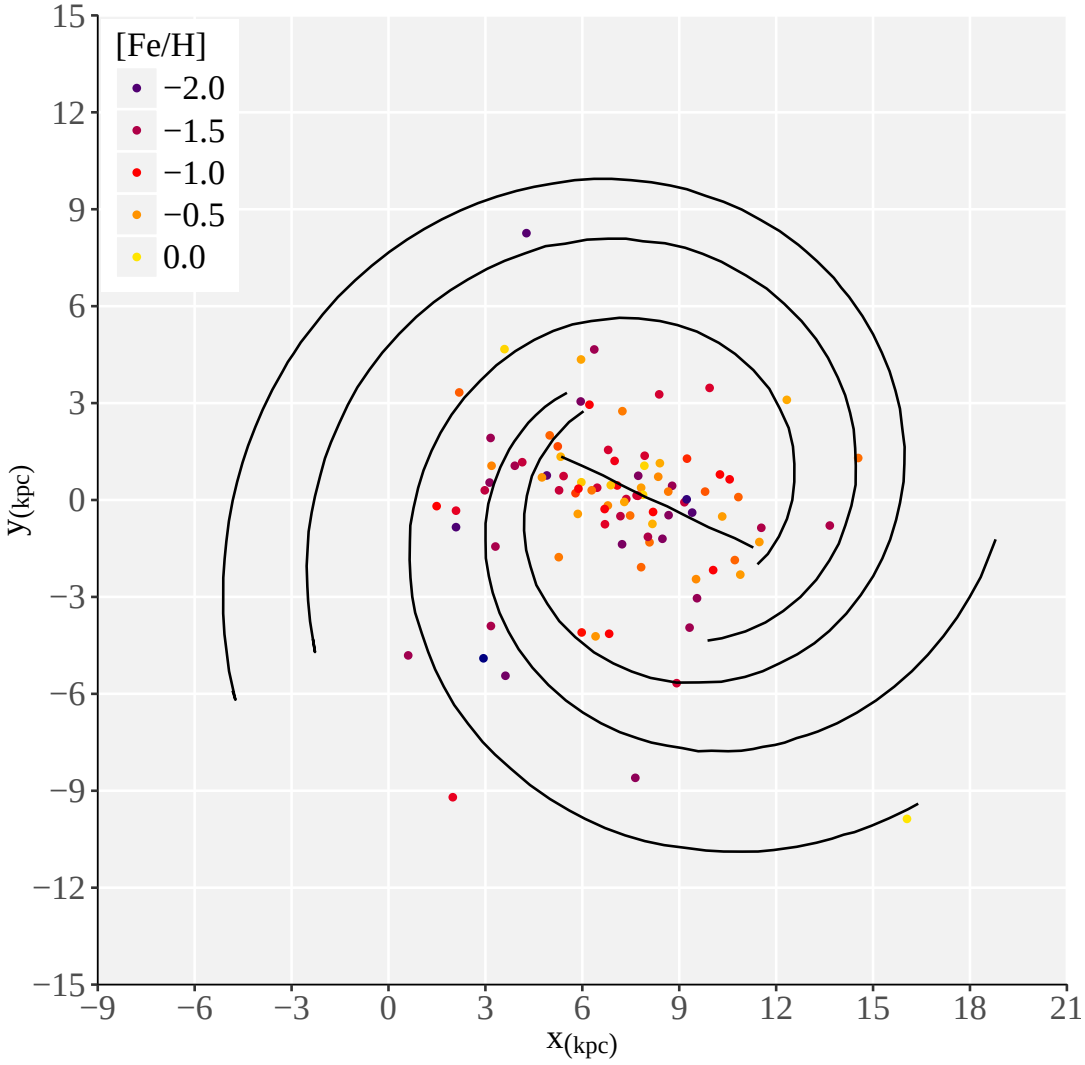

Figure 13 – Projection in the x, y plane of GCs with $|z| \leq 2.5$ kpc, superposed with the Galactic bar and spiral arms model of Russeil (2003). The GCs are color coded according to their metallicity as shown in the legend in the upper left corner.

error merely puts the GCs closer to or further away from the Sun without a significant spread even for unrealistic large values of α. To simulate a differential error, we assigned a random α for each GC distance and repeated the PPMCC

process. For a range $\alpha \in [0.5, 1.5]$, statistically significant correlations happened in 38% of 1000 cases. For $\alpha \in [0.7, 1.3]$, the figure was 73%, and for $\alpha \in [0.8, 1.2]$, 91%.

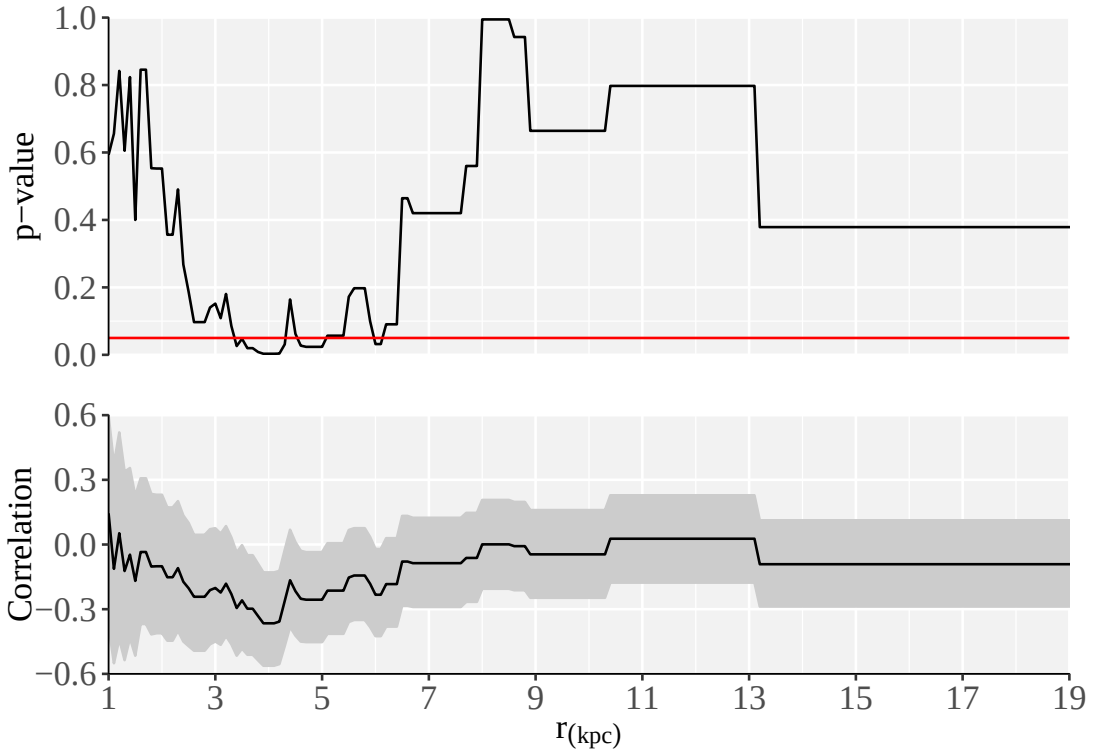

Figure 14 – Results of the PPMCC for the low height GCs inside a radius r. *Top:*p-values for varying r. The red line marks a p-value of 0.05. *Bottom:* The corresponding correlation coefficient, with a 95% confidence interval (grey).

7.5 Dynamical Simulations

While the presence of GCs near the plane of the disk grouped in an apparent bar structure was statistically significant, we performed orbit simulations to better understand if their current arrangement is maintained over a period of time or if it is a transient effect. For such, we employed the GALPY library for PYTHON (Bovy, 2015). We used the MWPOTENTIAL2014 potential, described in detail in

the aforementioned work. It considers a Hernquist bulge with cut-off at a radial distance of 1.9 kpc, a Miyamoto-Nagai disk, a Navarro–Frenk–White dark matter halo, and $R_0 = 8.0$ kpc. The spiral arms and the bar itself were not included. Our orbit integrations were over a period of 4.5 Gyr.

Statistically relevant correlations appear in a few non-continuous times but the bar structure dissolves within the first half Gyr. A bar rotates rigidly, therefore the observed scatter is a strong counter-evidence for its existence. The SDP also disappears with time, suggesting the higher density of GCs in that region could be temporary. However, the structure dissolution for both the SDP and the GC bar could be due to the uncertainties in the spatial velocity measurements, or the simplified potential model that does not include spiral arms or the known Galactic bar, both of which could have an important role in the central kiloparsecs relevant to this study. Several orbits remain within tight limits (Figs. 16, 17, and 18), close to the disk and within a small radius from the Galactic centre. Therefore, more tests are necessary to both understand how these structures came to exist in the present, and how they will evolve with time.

On a bigger scale, it appears that the centroid of the GC distribution changes with time, with the centroid of the low height GCs remaining mostly stable (Fig. 15). Fluctuations in the distance between the centroid and the centre of the potential are expected since the GC sample that possesses spatial velocity information is very small. However, this result offers an explanation as to why the centre of the GC system could be shifted from the centre of the Galaxy.

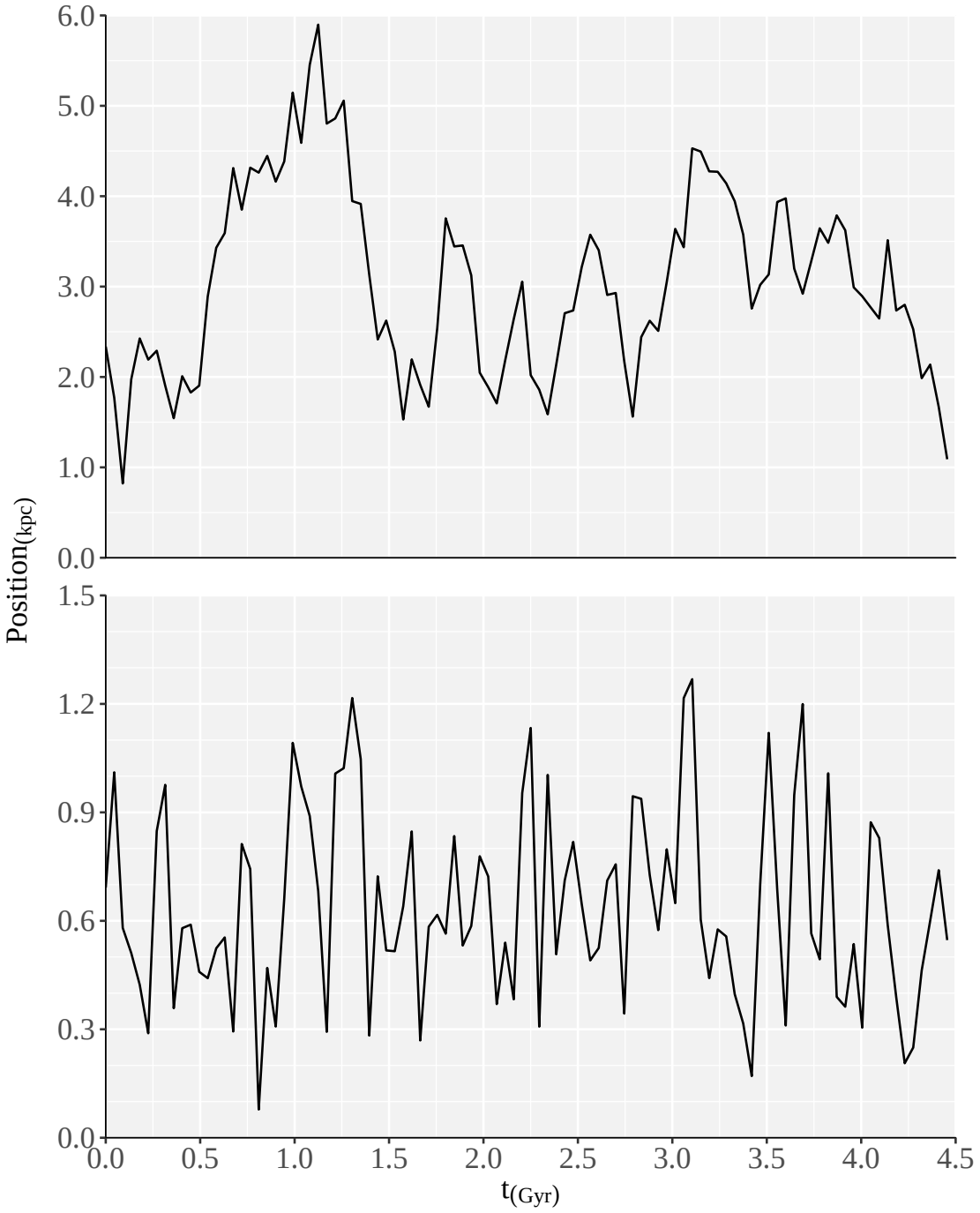

Figure 15 – Distance between the centroid of the GC system and the centre of the Galactic potential for the full sample (top), and the low height sample ($|z| \leq 2.5$ kpc, bottom).

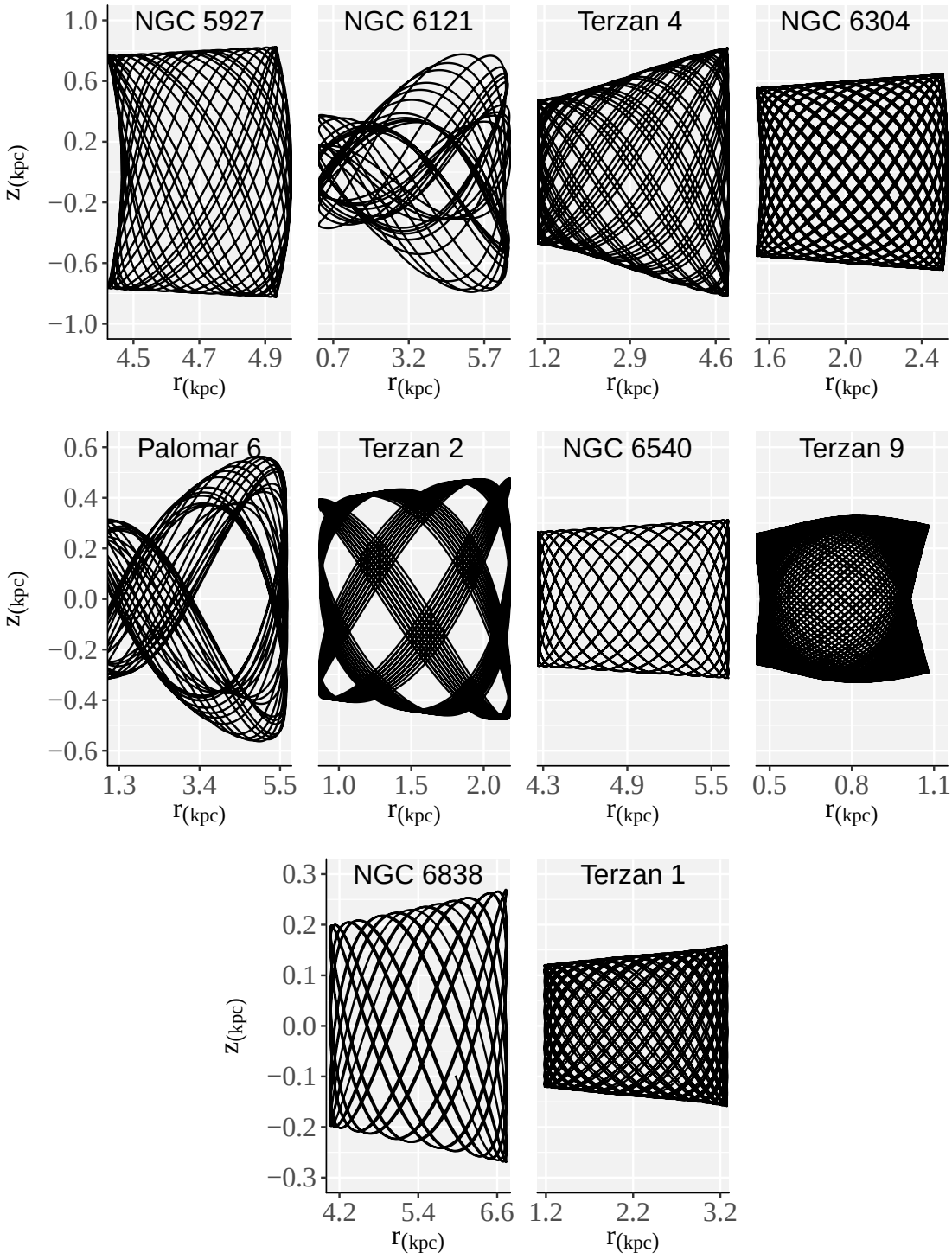

Figure 16 – Orbit projections in the z and r directions, where r is zero in the centre of the potential. The orbits were traced for 1.5 Gyr. Objects in this panel were always within $1kpc$ of the plane of the disk.

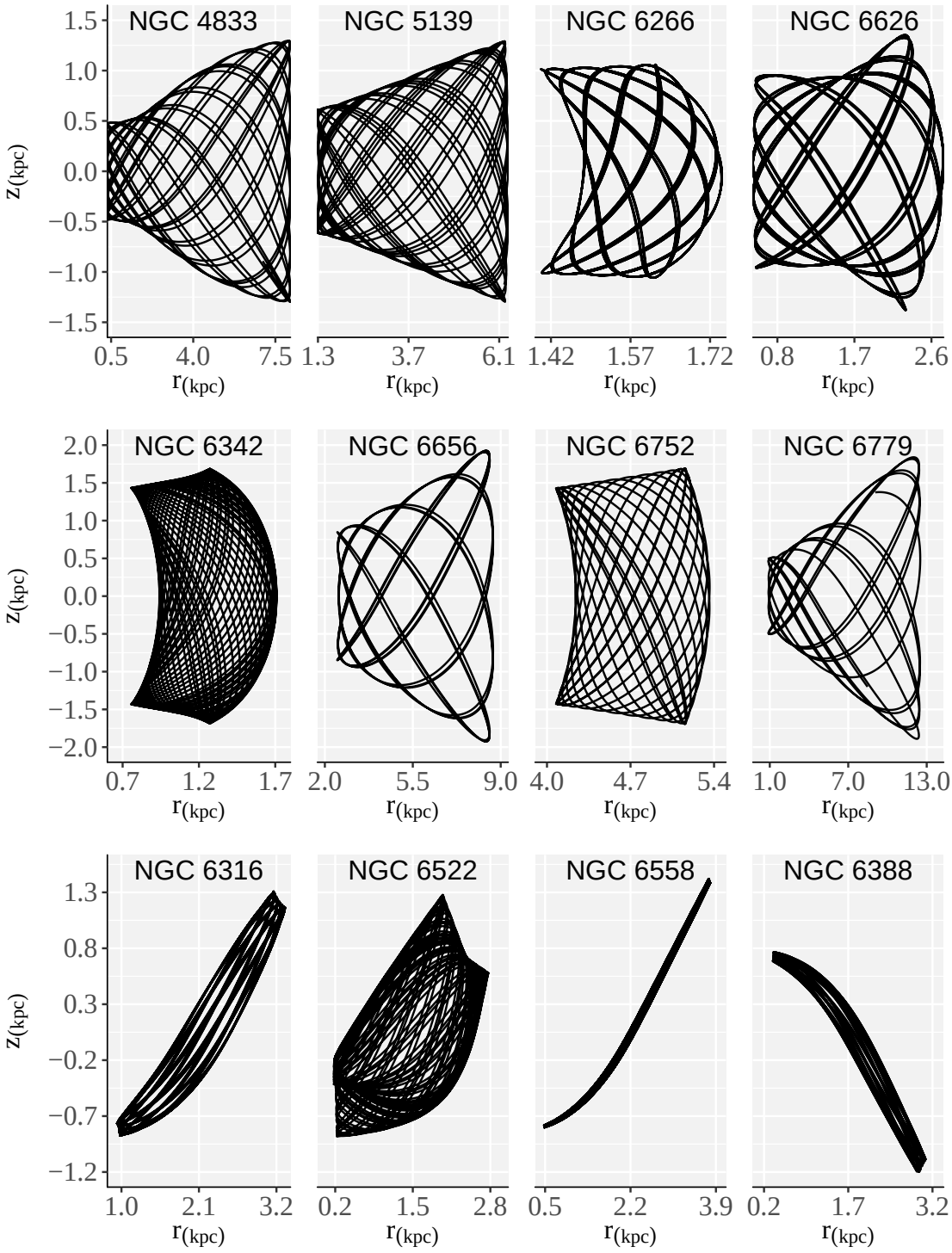

Figure 17 – Same as Fig. 16, but with objects which were always within $2kpc$ of the plane of the disk.

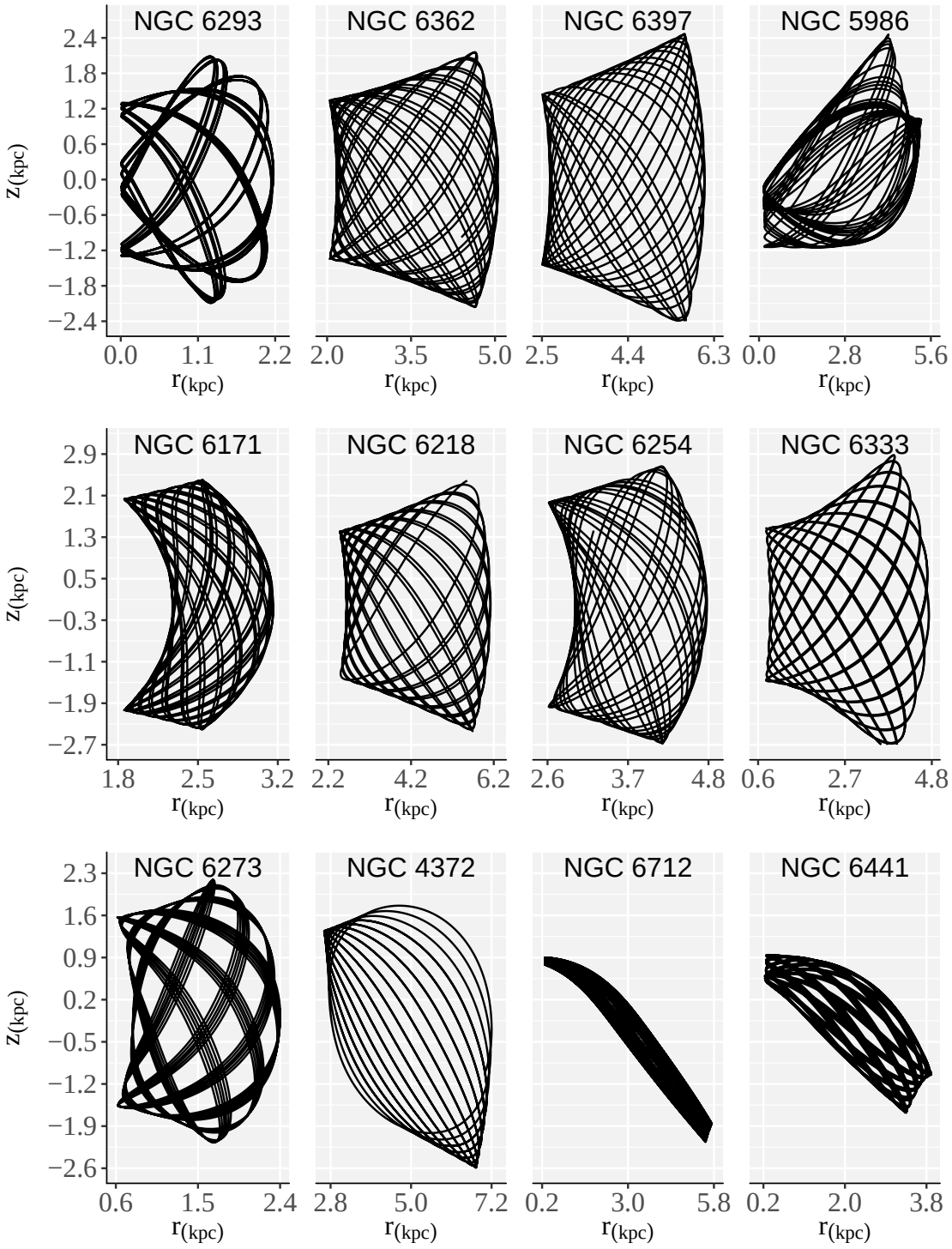

Figure 18 – Same as Fig. 16, but with objects which were always within $3kpc$ of the plane of the disk. Note that NGC 5986, NGC 6712, and NGC 6441 have asymmetrical orbits and remain closer to the disk than the rest of the sample in this figure.

8 Discussion

8.1 Centroid of the GC Distribution

As discussed by Reid (1993), each method for the determination of Galactic distances has its own constraints, often created by the formation and evolution models on which they are based. Despite geometrical distributions being relatively free of such dependencies, the methods for the determination of the GC distances themselves are not, which might create systematic errors in the determination of y_0, z_0, and specially x_0. The determination of distance uncertainties is tightly connected to the depth and resolution of CMDs, the quality of the available extinction maps, and to our understanding of the extinction curve (Sect. 3). Dust clouds with their particular compositions can be seen in the line of sight of several GCs (Sect. 3.1). Some authors do not present uncertainties, or are unclear about how they arrived in their values (e.g. using an extinction map, or directly from the observed CMD).

The centroid of the full sample lies at $(7.41 \pm 0.01, 0.11 \pm 0.02, 0.01 \pm 0.04)$ kpc (Tab. 7). This results in a distance to the centre of the GC distribution of 7.41 ± 0.01 kpc. While this value is lower than most recently derived values of R_0, it is in agreement with Francis & Anderson (2014), who used the GC distribution with the recalibrated RR Lyrae scale to determine the GC distances.

Recently, the VVV Survey discovered a new GC in the bulge: VVV CL002, and the still ambiguous candidate VVV CL003 (Moni Bidin et al., 2011). With these findings, we can presume that there may be considerably more GCs beyond the current detection limits, specially in the highly obscured region of the bar-like structure. Moni Bidin et al. (2011) estimated that at least 10 new GCs may still have their existence confirmed towards the bulge and disk. If they were concentrated in the far side of the bar, this number could be sufficient to bring x_0 closer to values for R_0 derived via other methods. It is important to note that this would still result in a x direction distribution markedly wider and shorter than in the y and z directions.

Assuming that the number of missing GCs in the far side of the bar is not significant, an interesting point is the analysis of reasons why the Galactic centre and the GC centroid would not coincide. The high destruction rate of GCs in the inner ≈ 2 kpc of the Galactic centre could explain a loss of symmetry in the GC distribution in that region. Another possibility is that the sample of GCs is small enough that its centroid oscillates with time, an hypothesis supported by our tests (Fig. 15). The biggest shifts from the centre of the potential happen for GCs that are far from the plane of the disk. Most GCs with recorded spatial velocities are near the Sun, thus the centroid oscillation could become more prominent if we included further away GCs in dynamical studies.

8.2 Effects of Small Sample Size

The Milky Way hosts a relatively small GC population. It is important to investigate if asymmetries such as the SDP and the apparent elongation near the x direction (Sect. 7.4.1) are produced because of a small sample size instead of a physical phenomenon. We created samples of 170 random x, y coordinates from a Gaussian distribution defined by the μ, σ parameters, and repeated the process described in the aforementioned section with a rotating k axis. As expected, the variety of distribution shapes for different values of θ is greater for a larger σ.

One of the samples is presented in Fig. 19. It was chosen because it mimics the secondary peak in a wider distribution for a certain value of θ, with a taller and narrower shape for another. This example shows that great care must be taken when attributing physical meaning to statistics of small numbers. In such cases, further investigation is necessary, such as plane projections matched to real structures (Fig. 13) or dynamical analyses (Sect. 7.5).

8.3 Structures

The SDP is mostly populated by low metallicity GCs (Fig. 10). With exclusively low height GCs ($|z| < 2.5$ kpc), we can verify the proximity between the SDP region and the spiral arms. The plane projection in Fig. 13 only shows

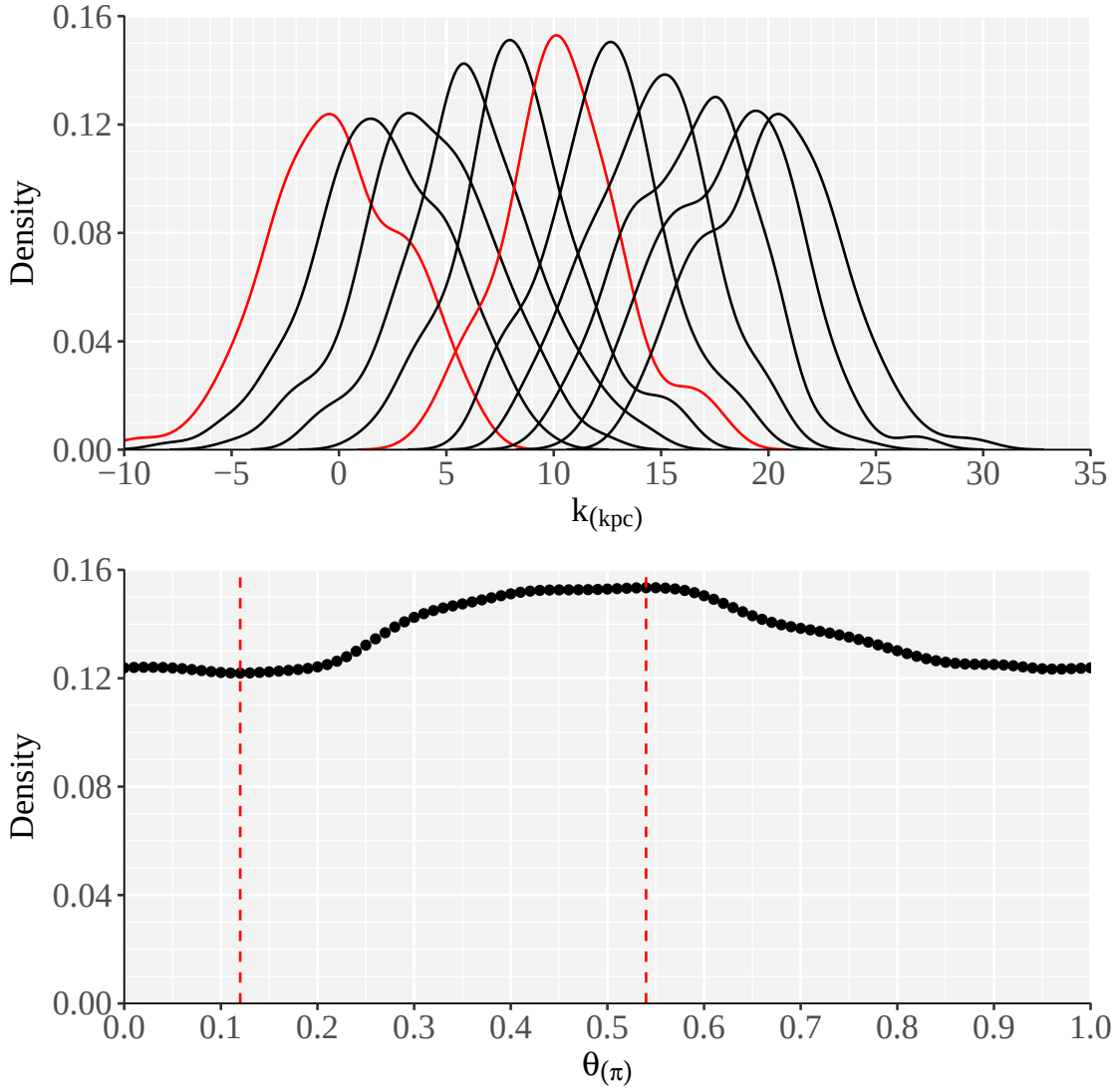

Figure 19 – *Top:* Density distribution in the k direction for 170 x, y coordinates randomly generated from a Gaussian distribution with $\mu = 0, \sigma = 3$. Each new k shifted 2 kpc to the right for clarity. In red, the $\theta = 0$ and $\pi/2$ directions. *Bottom:* The peaks of the k direction distribution for each θ for the same sample. The red dashed lines indicate the maximum and minimum values. Compare with Fig. 12.

GCs close to the disk and, consequently, the spiral arms of the Galaxy. The low height GCs in the SDP region are visibly close to the Scutum-Crux spiral arm, and might have their orbits disturbed by it. The exact position of each arm is still

Table 9 – Limits of the orbits of SDP GCs relative to the centre of the potential. The uncertainties were derived by running the simulations for the maximum and minimum spatial velocity values according to their own uncertainties (Tab. 3). Note that two GCs in this table are not in the low height subgroup, namely NGC 4372 and NGC 6254.

Name	R_{min}	R_{max}	$\|z\|_{max}$
NGC 4372	$2.76\pm^{0.32}_{0.75}$	$7.25\pm^{2.31}_{0.42}$	$2.57\pm^{0.58}_{0.00}$
NGC 4833	$0.34\pm^{0.08}_{0.08}$	$8.22\pm^{0.29}_{0.24}$	$1.29\pm^{0.23}_{0.14}$
NGC 5139	$1.31\pm^{0.03}_{0.02}$	$6.39\pm^{0.04}_{0.02}$	$1.30\pm^{0.02}_{0.01}$
NGC 6121	$0.22\pm^{0.08}_{0.08}$	$6.57\pm^{0.00}_{0.00}$	$0.79\pm^{0.04}_{0.03}$
NGC 6254	$2.99\pm^{0.67}_{0.59}$	$4.96\pm^{0.05}_{0.03}$	$2.69\pm^{0.28}_{0.22}$
NGC 6397	$2.68\pm^{0.12}_{0.13}$	$6.16\pm^{0.01}_{0.00}$	$2.47\pm^{0.02}_{0.02}$
NGC 6656	$2.56\pm^{0.12}_{0.13}$	$8.74\pm^{0.48}_{0.42}$	$1.97\pm^{0.18}_{0.17}$
NGC 6752	$4.23\pm^{0.23}_{0.24}$	$5.42\pm^{0.09}_{0.08}$	$1.68\pm^{0.02}_{0.00}$
NGC 6838	$4.06\pm^{0.06}_{0.10}$	$6.74\pm^{0.06}_{0.00}$	$0.26\pm^{0.02}_{0.00}$

under debate, and their total number as well. In our dynamical simulations, which did not include spiral arms nor the bar, many of the SDP GCs (Tab. 6) remain close to the disk and within 7.5 kpc of the potential centre. They are presented on Tab. 9 alongside the limits of their orbits in terms of maximum (R_{max}) and minimum (R_{min}) distance from the centre of the potential, and maximum distance from the plane of the disk $|z|_{max}$.

GCs are old objects that probably predate the formation of the Galactic disk. Yet many of them present low height orbits, some extremely so (Fig. 16), suggesting that the disk has been able to modify their orbits without destroying them altogether, including in the inner regions where the bulge, bar and spiral arms present a hostile environment for GC survival. Indeed, their disk crossing might even initiate star formation (Kobulnicky et al., 2005) and perhaps even form open clusters (Salerno et al., 2009). The high destruction rates in such areas suggest that the nearby GCs might have been significantly more massive in the past. NGC 5139 (ω Centauri), an object that is recognized as the remnant of an accreted galaxy, is one of the objects that remains tightly close to the disk and is present in the SDP (Fig. 17). Despite its extragalactic origin, this GC appears to have been trapped near the plane of the disk.

A bar-like structure of GCs is conspicuous in the xy plane (Fig. 13). The tilt of the bar is defined as the angle between the bar and the line of sight. With the GCs superposed on the spiral arm and bar model of Russeil (2003) it can be seen that a tilt of the GC conglomeration in the region is smaller than the value adopted for the Galactic bar by the aforementioned work. Indeed, Gerhard (2002) made a review of the studies of the Galactic bar and found that different tracers point to different values for the bar orientation, ranging from 15° to 30°. The ranges found for the GC bar-like structure for several radii were within this interval (Sect. 7.4.2).

It is also possible that the Galaxy presents a structural feature similar to that observed in the Large Magellanic Cloud: a main bar with a large age spread and a secondary bar, with an angular displacement of $22° \pm 2°$ relative to the first, with mainly young objects (Dottori et al., 1996). Therefore, we might be observing a bar-like structure populated mostly by GCs, which are old objects, displaced from the main Galactic bar which includes younger components.

While presently the bar-like structure is visually evident, the same does not happen for future ages in our dynamical simulations. The SDP might also be a transient effect. This could be due to the uncertainties, which greatly increase with the number of integrations, or to the adopted Galactic model that did not include a bar or spiral arms, which might be the key to the formation of such structures. Moreno, Pichardo & Velázquez (2014) found evidence that the presence of a bar decreases the bulge-shocking destruction rates. Allen, Moreno & Pichardo (2008) found that the presence of a bar, even a temporary one, causes larger vertical and radial distances with far more irregular orbits, and is capable of causing temporary reversal of the direction of orbital rotation for some objects. The latter work also concluded that spiral arms caused significant changes in the form of the orbits, even for small perturbations, though the bar dominates long-term effects.

Regardless of the length of the SDP and bar-like structure lifetime, it is important to understand why they exist in the present. The SDP is very close to the Sun and unlikely to contain objects with large errors. Over- or underestimation of GC distances as a whole does not significantly influence the bar-like structure, even for unrealistically large error factors, as it merely puts them closer or further away in the x direction while barely changing the y direction. It bears questioning

if differential distance over- or underestimation could dissolve the structure. We performed the same PPMCC test (Sect. 7.4.2) illustrated in Fig. 14 and found that for random errors of up to ±20% statistically significant correlations still happened in 91% of cases. This resulting value of 20% is higher than most found in the literature (Sect. 5).

9 Conclusions

The sample of GCs has increased since H10, from 157 to 170 in the present study. We employed the sample in a structural investigation of the Galaxy. We used distribution functions and fitted Sérsic profile functions to determine the centroids of their spatial distribution and identify asymmetries. We found that the centroid of the GC distribution lies at $(7.41 \pm 0.01, 0.11 \pm 0.02, 0.01 \pm 0.04)$ kpc in a cartesian coordinate system where the x direction points towards the Galactic centre, resulting in a distance of 7.41 ± 0.01 kpc from the Sun. This value is lower than the recent values for R_0, usually in the range 8 to 8.5 kpc. Using dynamical simulations for 68 GC with known spatial velocity, we found evidence that the centroid of their distribution oscillates with time, maybe because of their small sample number. This could explain why their centroid does not coincide with the centre of the Milky Way in the present.

Many of the known low height ($|z| < 2.5$ kpc) GCs are concentrated in a bar-like structure, with the possibility of undiscovered GCs on its far side. This structure is very likely to persist even with the application of an error of up to 20% in the GC distance values, where each GC is assigned a randomly generated distance error in this range. We detected an overdensity (SDP region) of GCs at $x \approx 3$ kpc from the Sun, in the direction of the Galactic centre. This overdensity is populated by mostly low metallicity GCs.

Neither the SDP nor the bar-like structure survive long in our dynamical simulations, quickly dissolving before the first half billion years. Since our models do not include a bar or spiral arms, simulations with these features are necessary to study these two structures. Even if they are short-lived, it is important to understand how they came to exist in the present and how the bar and spiral arms might affect the orbits of, or even capture, GCs. Several GCs appear to have orbits close to the disk and within the Solar orbit radius, including NGC 5139 (ω Centauri), which is known to have extragalactic origins. This shows that even accreted objects can have their orbits greatly influenced. The system is so dynamically evolved that

spatial analysis of the current sample is unable to differentiate between a monolithic collapse and a hierarchical accretion of satellites as the formation scenario of the Galaxy.

Using statistical methods applied to the available sample of GCs, we concluded that the quality of observations is in general very good, leading to small distance uncertainties. Based on this, we were able to make inferences about the GC system structure, and how it relates to the Galactic structure itself. Using dynamical simulations, we have offered an explanation as to why the centroid of the GC system does not coincide with the Galactic centre.

Future efforts should include new detections of GCs, specially beyond the Galactic centre, as well as Gaia improvements for distances and proper motions. More realistic Galactic potential models are necessary for the study of the bar-like structure and the interaction of GCs with the spiral arms. Comparison with extragalactic systems, which are constantly improving, can help us understand the formation history and current structure of the Milky Way.

Bibliography

Aguilar, L.; Hut, P.; Ostriker, J. P. On the evolution of globular cluster systems. I - Present characteristics and rate of destruction in our Galaxy. *Astrophysical Journal*, v. 335, p. 720–747, Dec. 1988.

Allen, C.; Moreno, E.; Pichardo, B. Six New Galactic Orbits of Globular Clusters in a Milky Way-Like Galaxy. *The Astrophysical Journal*, v. 674, p. 237–246, Feb. 2008.

Alonso-García, J. et al. Variable Stars in the VVV Globular Clusters. I. 2MASS-GC 02 and Terzan 10. *The Astronomical Journal*, v. 149, p. 99, Mar. 2015.

Arce, H. G.; Goodman, A. A. Measuring Galactic Extinction: A Test. *The Astrophysical Journal*, v. 512, p. L135–L138, Feb. 1999.

Baade, W. The Resolution of Messier 32, NGC 205, and the Central Region of the Andromeda Nebula. *Astrophysical Journal*, v. 100, p. 137, Sep. 1944.

Balbinot, E. et al. A New Milky Way Halo Star Cluster in the Southern Galactic Sky. *Astrophysical Journal*, v. 767, p. 101, Apr. 2013.

Bastian, N. A critical assessment of models for the origin of multiple populations in globular clusters. *ArXiv e-prints*, Oct. 2015.

Bedin, L. R. et al. The double main sequence of Omega Centauri. *Memorie della Societa Astronomica Italiana Supplementi*, v. 5, p. 105, 2004.

Bica, E. et al. Globular cluster system and Milky Way properties revisited. *Astronomy & Astrophysics*, v. 450, p. 105–115, Apr. 2006.

Bica, E.; Ortolani, S.; Barbuy, B. Globular Clusters in the Galactic Bulge. *Publications of the Astronomical Society of Australia*, v. 33, p. e028, Jun. 2016.

Bonatto, C. et al. Further probing the nature of FSR1767. *Monthly Notices of the Royal Astronomical Society*, v. 397, p. 1032–1040, Aug. 2009.

Bovy, J. galpy: A python Library for Galactic Dynamics. *The Astrophysical Journal Supplement Series*, v. 216, p. 29, Feb. 2015.

Cannon, R. D.; Stobie, R. S. Photometry of southern globular clusters I. Bright stars in omega Centauri. *Monthly Notices of the Royal Astronomical Society*, v. 162, p. 207, 1973.

Cardelli, J. A.; Clayton, G. C.; Mathis, J. S. The relationship between infrared, optical, and ultraviolet extinction. *Astrophysical Journal*, v. 345, p. 245–256, Oct. 1989.

Carraro, G.; Zinn, R.; Moni Bidin, C. Whiting 1: the youngest globular cluster associated with the Sagittarius dwarf spheroidal galaxy. *Astronomy and Astrophysics*, v. 466, p. 181–189, Apr. 2007.

Casetti-Dinescu, D. I. et al. Space Velocities of Southern Globular Clusters. V. A Low Galactic Latitude Sample. *The Astronomical Journal*, v. 134, p. 195–204, Jul. 2007.

Casetti-Dinescu, D. I. et al. Space Velocities of Southern Globular Clusters. VII. NGC 6397, NGC 6626 (M28), and NGC 6656 (M22). *The Astronomical Journal*, v. 146, p. 33, Aug. 2013.

Casetti-Dinescu, D. I. et al. Space Velocities of Southern Globular Clusters. VI. Nine Clusters in the Inner Milky Way. *The Astronomical Journal*, v. 140, p. 1282–1293, Nov. 2010.

Cohen, J. G. Abundances in globular cluster red giants. I - M3 and M13. *Astrophysical Journal*, v. 223, p. 487–508, Jul. 1978.

D'Antona, F. et al. A Helium Spread among the Main-Sequence Stars in NGC 2808. *Astrophysical Journal*, v. 631, p. 868–878, Oct. 2005.

Davies, B. et al. GLIMPSE-CO1: the most massive intermediate-age stellar cluster in the Galaxy. *Monthly Notices of the Royal Astronomical Society*, v. 411, p. 1386–1394, Feb. 2011.

Davoust, E.; Sharina, M. E.; Donzelli, C. J. The globular cluster BH 176 revisited. *Astronomy & Astrophysics*, v. 528, p. A70, Apr. 2011.

Dékány, I. et al. VVV Survey Near-infrared Photometry of Known Bulge RR Lyrae Stars: The Distance to the Galactic Center and Absence of a Barred Distribution of the Metal-poor Population. *Astrophysical Journal, Letters*, v. 776, p. L19, Oct. 2013.

Di Criscienzo, M. et al. A New Census of the Variable Star Population in the Globular Cluster NGC 2419. *The Astronomical Journal*, v. 141, p. 81, Mar. 2011.

Dinescu, D. I.; Girard, T. M.; van Altena, W. F. Space Velocities of Globular Clusters. III. Cluster Orbits and Halo Substructure. *The Astronomical Journal*, v. 117, p. 1792–1815, Apr. 1999.

Dinescu, D. I. et al. Space Velocities of Southern Globular Clusters. IV. First Results for Inner Galaxy Clusters. *The Astronomical Journal*, v. 125, p. 1373–1382, Mar. 2003.

Dinescu, D. I. et al. The Absolute Proper Motion of Palomar 12: A Case for Tidal Capture from the Sagittarius Dwarf Spheroidal Galaxy. *The Astronomical Journal*, v. 120, p. 1892–1905, Oct. 2000.

Dotter, A. et al. The ACS Survey of Galactic Globular Clusters. II. Stellar Evolution Tracks, Isochrones, Luminosity Functions, and Synthetic Horizontal-Branch Models. *The Astronomical Journal*, v. 134, p. 376–390, Jul. 2007.

Dottori, H. et al. Spatial Distributions of Young Large Magellanic Cloud Clusters as Tracers of a Bar Perturbation. *Astrophysical Journal*, v. 461, p. 742, Apr. 1996.

Dunlop, J. A Catalogue of Nebulae and Clusters of Stars in the Southern Hemisphere, Observed at Paramatta in New South Wales. *Philosophical Transactions*, v. 118, p. 113–151, Jan. 1828.

Dutra, C. M.; Bica, E. A catalogue of dust clouds in the Galaxy. *Astronomy and Astrophysics*, v. 383, p. 631–635, Feb. 2002.

Dutra, C. M.; Santiago, B. X.; Bica, E. Low-extinction windows in the inner Galactic Bulge. *Astronomy & Astrophysics*, v. 381, p. 219–226, Jan. 2002.

Eggen, O. J.; Lynden-Bell, D.; Sandage, A. R. Evidence from the motions of old stars that the Galaxy collapsed. *Astrophysical Journal*, v. 136, p. 748, Nov. 1962.

Ferraro, F. R. et al. The Giant, Horizontal, and Asymptotic Branches of Galactic Globular Clusters. I. The Catalog, Photometric Observables, and Features. *The Astronomical Journal*, v. 118, p. 1738–1758, Oct. 1999.

Fitzpatrick, E. L.; Massa, D. An Analysis of the Shapes of Interstellar Extinction Curves. V. The IR-through-UV Curve Morphology. *The Astrophysical Journal*, v. 663, p. 320–341, Jul. 2007.

Foster, T.; Cooper, B. Structure and Dynamics of the Milky Way: The Evolving Picture. In: Kothes, R.; Landecker, T. L.; Willis, A. G. (Ed.). *The Dynamic Interstellar Medium: A Celebration of the Canadian Galactic Plane Survey*. [S.l.: s.n.], 2010. (Astronomical Society of the Pacific Conference Series, v. 438), p. 16.

Francis, C.; Anderson, E. Two estimates of the distance to the Galactic Centre. *Monthly Notices of the Royal Astronomical Society*, v. 441, p. 1105–1114, Jun. 2014.

Gerhard, O. The Galactic Bar. In: Da Costa, G. S.; Sadler, E. M.; Jerjen, H. (Ed.). *The Dynamics, Structure & History of Galaxies: A Workshop in Honour of Professor Ken Freeman*. [S.l.: s.n.], 2002. (Astronomical Society of the Pacific Conference Series, v. 273), p. 73.

Gratton, R.; Sneden, C.; Carretta, E. Abundance Variations Within Globular Clusters. *Annual Review of Astronomy & Astrophysics*, v. 42, p. 385–440, Sep. 2004.

Gratton, R. G.; Carretta, E.; Bragaglia, A. Multiple populations in globular clusters. Lessons learned from the Milky Way globular clusters. *The Astronomy and Astrophysics Review*, v. 20, p. 50, Feb. 2012.

Hanes, D. A.; Madore, B. F. (Ed.). *Globular Clusters (Cambridge Astrophysics)*. 1. ed. [S.l.]: Cambridge University Press, 1980. ISBN 9780521228619.

Harris, W. E. A Catalog of Parameters for Globular Clusters in the Milky Way. *The Astronomical Journal*, v. 112, p. 1487, Oct. 1996.

Herschel, W. Catalogue of a Second Thousand of New Nebulae and Clusters of Stars; With a Few Introductory Remarks on the Construction of the Heavens. By William Herschel, L L. D. F. R. S. *Philosophical Transactions of the Royal Society of London Series I*, v. 79, p. 212–255, 1789.

Hertzsprung, E. Number 63. Zweiundzwanzigsten Bandes Erstes Stuck. Uber die verwendung photographischer effecktiver wellenlangen zur bestimmung von farbenaquivalenten. *Publikationen des Astrophysikalischen Observatoriums zu Potsdam*, v. 22, p. A1–A40.1, 1911.

Ibata, R. A.; Gilmore, G.; Irwin, M. J. A dwarf satellite galaxy in Sagittarius. *Nature*, v. 370, p. 194–196, Jul. 1994.

Ibata, R. A. et al. The Kinematics, Orbit, and Survival of the Sagittarius Dwarf Spheroidal Galaxy. *The Astronomical Journal*, v. 113, p. 634–655, Feb. 1997.

Ivanov, V. D.; Kurtev, R.; Borissova, J. Red giant branch stars as probes of stellar populations. II. Properties of the newly discovered globular cluster GLIMPSE-C01. *Astronomy & Astrophysics*, v. 442, p. 195–200, Oct. 2005.

Kalirai, J. S. et al. The Space Motion of the Globular Cluster NGC 6397. *The Astrophysical Journal Letters*, v. 657, p. L93–L96, Mar. 2007.

Kim, D.; Jerjen, H. A Hero's Little Horse: Discovery of a Dissolving Star Cluster in Pegasus. *Astrophysical Journal*, v. 799, p. 73, Jan. 2015.

Kim, D. et al. KIM 3: An Ultra-faint Star Cluster in the Constellation of Centaurus. *The Astrophysical Journal*, v. 820, p. 119, Apr. 2016.

Kim, D. et al. Discovery of a Faint Outer Halo Milky Way Star Cluster in the Southern Sky. *Astrophysical Journal*, v. 803, p. 63, Apr. 2015.

Kirby, E. N.; Simon, J. D.; Cohen, J. G. Spectroscopic Confirmation of the Dwarf Galaxies Hydra II and Pisces II and the Globular Cluster Laevens 1. *Astrophysical Journal*, v. 810, p. 56, Sep. 2015.

Kobulnicky, H. A. et al. Discovery of a New Low-Latitude Milky Way Globular Cluster Using GLIMPSE. *The Astronomical Journal*, v. 129, p. 239–250, Jan. 2005.

Laevens, B. P. M. et al. Sagittarius II, Draco II and Laevens 3: Three New Milky Way Satellites Discovered in the Pan-STARRS 1 3π Survey. *Astrophysical Journal*, v. 813, p. 44, Nov. 2015.

Laevens, B. P. M. et al. A New Distant Milky Way Globular Cluster in the Pan-STARRS1 3π Survey. *Astrophysical Journal, Letters*, v. 786, p. L3, May 2014.

Lee, J.-W. et al. Toward a Better Understanding of the Distance Scale from RR Lyrae Variable Stars: A Case Study for the Inner Halo Globular Cluster NGC 6723. *The Astrophysical Journal Supplement*, v. 210, p. 6, Jan. 2014.

Lin, D. N. C.; Richer, H. B. Young globular clusters in the Milky Way Galaxy. *Astrophysical Journal, Letters*, v. 388, p. L57–L60, Apr. 1992.

Longmore, A. J. et al. Mercer 5: a probable new globular cluster in the Galactic bulge. *Monthly Notices of the Royal Astronomical Society*, v. 416, p. 465–478, Sep. 2011.

Luque, E. et al. Digging deeper into the Southern skies: a compact Milky Way companion discovered in first-year Dark Energy Survey data. *Monthly Notices of the Royal Astronomical Society*, v. 458, p. 603–612, May 2016.

Lynden-Bell, D. Dwarf galaxies and globular clusters in high velocity hydrogen streams. *Monthly Notices of the Royal Astronomical Society*, v. 174, p. 695–710, Mar. 1976.

Lynden-Bell, D.; Lynden-Bell, R. M. Ghostly streams from the formation of the Galaxy's halo. *Monthly Notices of the Royal Astronomical Society*, v. 275, p. 429–442, Jul. 1995.

Malkin, Z. M. Analysis of determinations of the distance between the sun and the galactic center. *Astronomy Reports*, v. 57, p. 128–133, Feb. 2013.

Marín-Franch, A. et al. The ACS Survey of Galactic Globular Clusters. VII. Relative Ages. *The Astrophysical Journal*, v. 694, p. 1498–1516, Apr. 2009.

Marino, A. F. et al. The halo+cluster system of the Galactic globular cluster NGC 1851. *Monthly Notices of the Royal Astronomical Society*, v. 442, p. 3044–3064, Aug. 2014.

Marshall, D. J. et al. Modelling the Galactic interstellar extinction distribution in three dimensions. *Astronomy and Astrophysics*, v. 453, p. 635–651, Jul. 2006.

Martin, N. F. et al. A dwarf galaxy remnant in Canis Major: the fossil of an in-plane accretion on to the Milky Way. *Monthly Notices of the Royal Astronomical Society*, v. 348, p. 12–23, Feb. 2004.

Miles, R. A light history of photometry: from Hipparchus to the Hubble Space Telescope. *Journal of the British Astronomical Association*, v. 117, p. 172–186, Aug. 2007.

Milone, A. P. et al. The Hubble Space Telescope UV Legacy Survey of Galactic Globular Clusters. III. A Quintuple Stellar Population in NGC 2808. *The Astrophysical Journal*, v. 808, p. 51, Jul. 2015.

Milone, A. P. et al. Absolute motions of globular clusters. II. HST astrometry and VLT radial velocities in NGC 6397. *Astronomy and Astrophysics*, v. 456, p. 517–522, Sep. 2006.

Minniti, D. et al. Discovery of VVV CL001. A low-mass globular cluster next to UKS 1 in the direction of the Galactic bulge. *Astronomy & Astrophysics*, v. 527, p. A81, Mar. 2011.

Moni Bidin, C. et al. Three Galactic globular cluster candidates. *Astronomy & Astrophysics*, v. 535, p. A33, Nov. 2011.

Moreno, E.; Pichardo, B.; Velázquez, H. Tidal Radii and Destruction Rates of Globular Clusters in the Milky Way due to Bulge-Bar and Disk Shocking. *The Astrophysical Journal*, v. 793, p. 110, Oct. 2014.

Muñoz, R. R. et al. The Discovery of an Ultra-faint Star Cluster in the Constellation of Ursa Minor. *Astrophysical Journal, Letters*, v. 753, p. L15, Jul. 2012.

Nishiyama, S. et al. The Distance to the Galactic Center Derived from Infrared Photometry of Bulge Red Clump Stars. *The Astrophysical Journal*, v. 647, p. 1093–1098, Aug. 2006.

Odenkirchen, M. et al. Kinematics of the Tidal Debris of the Globular Cluster Palomar 5. *The Astronomical Journal*, v. 137, p. 3378–3387, Feb. 2009.

Ortolani, S. et al. Distances of the bulge globular clusters Terzan 5, Liller 1, UKS 1, and Terzan 4 based on HST NICMOS photometry. *Astronomy and Astrophysics*, v. 470, p. 1043–1049, Aug. 2007.

Ortolani, S.; Bica, E.; Barbuy, B. NTT V, I and Gunn Z colour-magnitude diagrams of Liller 1: a globular cluster as metal-rich as the inner bulge stellar population? *Astronomy & Astrophysics*, v. 306, p. 134, Feb. 1996.

Ortolani, S.; Bica, E.; Barbuy, B. Segue 3: the youngest globular cluster in the outer halo. *Monthly Notices of the Royal Astronomical Society*, v. 433, p. 1966–1969, Aug. 2013.

Ortolani, S. et al. The old open clusters Berkeley 36, Berkeley 73 and Biurakan 13 (Berkeley 34). *Astronomy and Astrophysics*, v. 429, p. 607–612, Jan. 2005.

Ortolani, S. et al. Pfleiderer 2: Identification of A New Globular Cluster in the Galaxy. *The Astronomical Journal*, v. 138, p. 889–894, Sep. 2009.

Ortolani, S. et al. Kronberger 49: A New Low-mass Globular Cluster or an Unprecedented Bulge Window? *The Astronomical Journal*, v. 144, p. 147, Nov. 2012.

Osborn, W. Two new CN-strong globular cluster stars. *The Observatory*, v. 91, p. 223–224, Dec. 1971.

Paust, N.; Wilson, D.; van Belle, G. Reinvestigating the Clusters Koposov 1 and 2. *The Astronomical Journal*, v. 148, p. 19, Jul. 2014.

Pawlowski, M. S.; Pflamm-Altenburg, J.; Kroupa, P. The VPOS: a vast polar structure of satellite galaxies, globular clusters and streams around the Milky Way. *Monthly Notices of the Royal Astronomical Society*, v. 423, p. 1109–1126, Jun. 2012.

Peñaloza, F. et al. Chemical Abundances of the Highly Obscured Galactic Globular Clusters 2MASS GC02 and Mercer 5. *Publications of the Astronomical Society of the Pacific*, v. 127, p. 329–339, Apr. 2015.

Piotto, G. et al. A Triple Main Sequence in the Globular Cluster NGC 2808. *Astrophysical Journal, Letters*, v. 661, p. L53–L56, May 2007.

Piotto, G. et al. Metallicities on the Double Main Sequence of ω Centauri Imply Large Helium Enhancement. *Astrophysical Journal*, v. 621, p. 777–784, Mar. 2005.

Pryor, C.; Piatek, S.; Olszewski, E. W. Proper Motion of the Sagittarius Dwarf Galaxy Based on Hubble Space Telescope Imaging. *The Astronomical Journal*, v. 139, p. 839–856, Mar. 2010.

Reid, M. J. The distance to the center of the Galaxy. *Annual Review of Astronomy & Astrophysics*, v. 31, p. 345–372, 1993.

Rossi, L. J. et al. Proper motions and kinematics of selected bulge globular clusters. *Monthly Notices of the Royal Astronomical Society*, v. 450, p. 3270–3288, Jul. 2015.

Russeil, D. Star-forming complexes and the spiral structure of our Galaxy. *Astronomy & Astrophysics*, v. 397, p. 133–146, Jan. 2003.

Salerno, G. M. et al. On the possible generation of the young massive open clusters Stephenson 2 and BDSB 122 by ω Centauri. *Astronomy and Astrophysics*, v. 498, p. 419–423, May 2009.

Salinas, R.; Strader, J. No Evidence for Multiple Stellar Populations in the Low-mass Galactic Globular Cluster E 3. *The Astrophysical Journal*, v. 809, p. 169, Aug. 2015.

Sawyer, H. B. A bibliography of individual globular clusters. *Publications of the David Dunlap Observatory*, v. 1, p. 381–469, Apr. 1949.

Schlegel, D. J.; Finkbeiner, D. P.; Davis, M. Maps of Dust Infrared Emission for Use in Estimation of Reddening and Cosmic Microwave Background Radiation Foregrounds. *The Astrophysical Journal*, v. 500, p. 525–553, Jun. 1998.

Searle, L.; Zinn, R. Compositions of halo clusters and the formation of the galactic halo. *Astrophysical Journal*, v. 225, p. 357–379, Oct. 1978.

Shapley, H. Studies based on the colors and magnitudes in stellar clusters. I. The general problem of clusters. *Contributions from the Mount Wilson Observatory / Carnegie Institution of Washington*, v. 115, 1916.

Shapley, H. Studies based on the colors and magnitudes in stellar clusters. VII. The distances, distribution in space, and dimensions of 69 globular clusters. *Astrophysical Journal*, v. 48, Oct. 1918.

Siegel, M. H. et al. A Cluster's Last Stand: The Death of Palomar 13. *The Astronomical Journal*, v. 121, p. 935–950, Feb. 2001.

Sollima, A. et al. Discovery of Tidal Tails Around the Distant Globular Cluster Palomar 14. *The Astrophysical Journal*, v. 726, p. 47, Jan. 2011.

Trumpler, R. J. Absorption of Light in the Galactic System. *Publications of the Astronomical Society of the Pacific*, v. 42, p. 214, Aug. 1930.

Turner, D. G. An eclectic view of our Milky Way galaxy. *Canadian Journal of Physics*, v. 92, p. 959–963, Sep. 2014.

Valenti, E.; Ferraro, F. R.; Origlia, L. Near-Infrared Properties of 24 Globular Clusters in the Galactic Bulge. *The Astronomical Journal*, v. 133, p. 1287–1301, Apr. 2007.

van den Bergh, S. The Luminosity Distribution of Globular Clusters in Dwarf Galaxies. *The Astronomical Journal*, v. 134, p. 344–345, Jul. 2007.

Villanova, S. et al. Ruprecht 106: The First Single Population Globular Cluster? *The Astrophysical Journal*, v. 778, p. 186, Dec. 2013.

Villanova, S. et al. The Multiplicity of the Subgiant Branch of ω Centauri: Evidence for Prolonged Star Formation. *The Astrophysical Journal*, v. 663, p. 296–314, Jul. 2007.

Watkins, L. L. et al. Hubble Space Telescope Proper Motion (HSTPROMO) Catalogs of Galactic Globular Clusters. III. Dynamical Distances and Mass-to-Light Ratios. *The Astrophysical Journal*, v. 812, p. 149, Oct. 2015.

Webbink, R. F. Structure parameters of galactic globular clusters. In: Goodman, J.; Hut, P. (Ed.). *Dynamics of Star Clusters*. [S.l.: s.n.], 1985. (IAU Symposium, v. 113), p. 541–577.

York, D. G. et al. The Sloan Digital Sky Survey: Technical Summary. *The Astronomical Journal*, v. 120, p. 1579–1587, Sep. 2000.

Zinn, R. The globular cluster system of the Galaxy. II - The spatial and metallicity distributions, the second parameter phenomenon, and the formation of the cluster system. *Astrophysical Journal*, v. 241, p. 602–617, Oct. 1980.